Article

Molecular Cell

PINK1 Phosphorylates MIC60/Mitofilin to Control Structural Plasticity of Mitochondrial Crista Junctions

Graphical Abstract

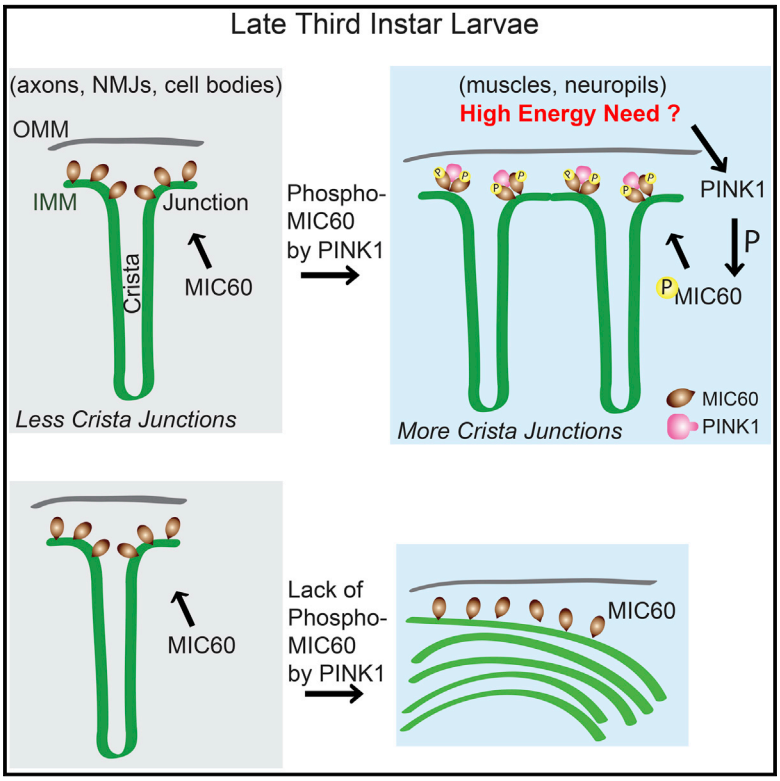

Highlights

- Mitochondria remodel crista junctions in selective subcellular areas in *Drosophila*
- This structural remodeling requires PINK1 to phosphorylate MIC60
- PINK1-mediated phosphorylation of MIC60 stabilizes MIC60 oligomerization
- Rare coding variants of *MIC60* found in Parkinson's patients are damaging in flies

Authors

Pei-I Tsai, Chin-Hsien Lin, Chung-Han Hsieh, ..., Michael D. Greicius, Owen A. Ross, Xinnan Wang

Correspondence

xinnanw@stanford.edu

In Brief

Tsai et al. discover that mitochondria increase crista junctions and numbers in selective subcellular areas in *Drosophila*. This structural remodeling requires Parkinson's-linked PINK1 to phosphorylate the inner mitochondrial membrane protein MIC60, which stabilizes MIC60 oligomerization. MIC60 functions downstream of PINK1 to maintain mitochondrial functions and cellular survival.

Tsai et al., 2018, Molecular Cell *69*, 744–756
March 1, 2018
https://doi.org/10.1016/j.molcel.2018.01.026

CellPress

CellPress

Molecular Cell
Article

PINK1 Phosphorylates MIC60/Mitofilin to Control Structural Plasticity of Mitochondrial Crista Junctions

Pei-I Tsai,[1] Chin-Hsien Lin,[2] Chung-Han Hsieh,[1] Amanda M. Papakyrikos,[1,3] Min Joo Kim,[1] Valerio Napolioni,[4] Carmen Schoor,[5] Julien Couthouis,[6] Ruey-Meei Wu,[2] Zbigniew K. Wszolek,[7] Dominic Winter,[5] Michael D. Greicius,[4] Owen A. Ross,[8] and Xinnan Wang[1,9,*]

[1]Department of Neurosurgery, Stanford University School of Medicine, Stanford, CA 94305, USA
[2]Department of Neurology, National Taiwan University Hospital, Taipei 100, Taiwan
[3]Graduate Program in Developmental Biology, Stanford University School of Medicine, Stanford, CA 94305, USA
[4]Functional Imaging in Neuropsychiatric Disorders (FIND) Lab, Department of Neurology and Neurological Sciences, Stanford University School of Medicine, Stanford, CA 94305, USA
[5]Institute for Biochemistry and Molecular Biology, University of Bonn, Bonn 53115, Germany
[6]Department of Genetics, Stanford University School of Medicine, Stanford, CA 94305, USA
[7]Department of Neurology, Mayo Clinic, Jacksonville, FL 32224, USA
[8]Department of Neuroscience, Mayo Clinic, Jacksonville, FL 32224, USA
[9]Lead Contact
*Correspondence: xinnanw@stanford.edu
https://doi.org/10.1016/j.molcel.2018.01.026

SUMMARY

Mitochondrial crista structure partitions vital cellular reactions and is precisely regulated by diverse cellular signals. Here, we show that, in *Drosophila*, mitochondrial cristae undergo dynamic remodeling among distinct subcellular regions and the Parkinson's disease (PD)-linked Ser/Thr kinase PINK1 participates in their regulation. Mitochondria increase crista junctions and numbers in selective subcellular areas, and this remodeling requires PINK1 to phosphorylate the inner mitochondrial membrane protein MIC60/mitofilin, which stabilizes MIC60 oligomerization. Expression of MIC60 restores crista structure and ATP levels of *PINK1*-null flies and remarkably rescues their behavioral defects and dopaminergic neurodegeneration. In an extension to human relevance, we discover that the PINK1-MIC60 pathway is conserved in human neurons, and expression of several *MIC60* coding variants in the mitochondrial targeting sequence found in PD patients in *Drosophila* impairs crista junction formation and causes locomotion deficits. These findings highlight the importance of maintenance and plasticity of crista junctions to cellular homeostasis *in vivo*.

INTRODUCTION

Efficient mitochondrial oxidative phosphorylation and ATP synthesis rely heavily on the exquisite membrane organization of the mitochondrial cristae. The inner mitochondrial membrane (IMM) protrudes into the matrix to form cristae that harbor the electron transport chain (ETC) machinery and ATP synthase. Each individual crista contains a tubular invagination, with an opening to the intermembrane space called crista junction and a bottom called crista tip (Figure 1A). Crista membranes bend extensively at crista junctions and tips to sustain the remarkably narrow and elongated crista space, and this unique shape is required for maintenance of solute gradients and localization of the ETC complexes (Mannella et al., 2013). Studies in yeast have revealed several crucial factors involved in maintenance of crista structure, including MIC60 (IMMT/Fcj1/mitofilin), mitochondrial fission-fusion machinery, F_oF_1-ATP synthase, and mdm33 (Frezza et al., 2006; Meeusen et al., 2006; Messerschmitt et al., 2003; Rabl et al., 2009; Strauss et al., 2008). MIC60 is an IMM integral protein and a major component of the mitochondrial contact site and cristae organizing system (MICOS) complex (Pfanner et al., 2014). Mitochondrial crista structure is not always static; instead, it undergoes dynamic remodeling tightly correlated with the mitochondrial aerobic respiration rates (Hackenbrock, 1966; John et al., 2005; Mannella et al., 2013). In high-energy-demanding cells, mitochondria perform higher respiratory activities. However, it remains elusive as to how cellular signals instruct mitochondria to remodel the crista architecture, particularly in an *in vivo* setting.

Mutations in the Ser/Thr kinase PINK1 cause autosomal recessive early-onset Parkinson's disease (PD) (Valente et al., 2004). The hallmark of PD is age-dependent degeneration of dopaminergic (DA) neurons in the substantia nigra. PINK1 is imported into healthy mitochondria with the polarized mitochondrial membrane potential ($\Delta\Psi m$) (Greene et al., 2012; Morais et al., 2014; Thomas et al., 2014). PINK1 is blocked from import into depolarized mitochondria and stabilized on the outer mitochondrial membrane (OMM), where it phosphorylates its substrates to trigger mitophagy (Chen and Dorn, 2013; Kondapalli et al., 2012; Narendra et al., 2008; Vives-Bauza and Przedborski, 2011; Wang et al., 2011; Whitworth and Pallanck, 2009).

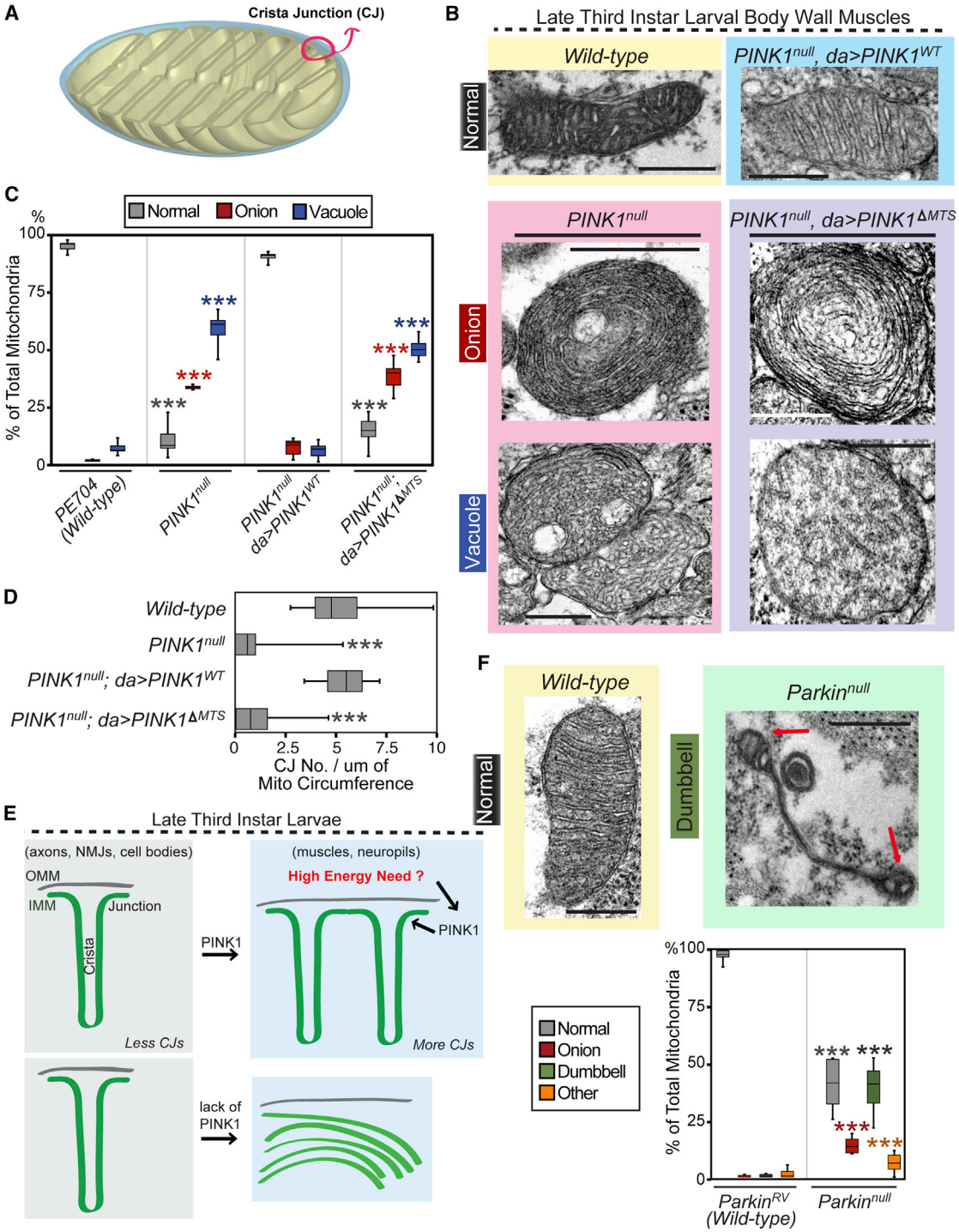

Figure 1. PINK1 Maintains Crista Junctions

(A) Cartoon depicting a mitochondrial crista junction (red circle).

(B and F) TEM images of body wall muscles of late third instar larvae (120 hr AEL) of *PINK1* null (B) or *Parkin* null (F).

(C and F) Quantification of the percentage of total mitochondria per image for *PINK1* null (C) or *Parkin* null (F). n = 307–916 mitochondria from 32–98 images obtained from 6–8 flies.

(D) Quantification of the number of crista junctions normalized to the length of the mitochondrial circumference. n = 30 mitochondria from 30 images from 6–8 flies.

(E) Schematic representation of PINK1-mediated plasticity of crista structure in third instar larvae.

(legend continued on next page)

However, whether PINK1 has kinase activity inside healthy mitochondria remains controversial. Although PINK1 has been shown to be crucial for the mitochondrial complex I activity, direct PINK1 kinase substrates in the ETC have not yet been identified (Morais et al., 2014; Pogson et al., 2014). In this work, we discover a novel substrate of PINK1 inside healthy mitochondria—the IMM protein MIC60, and reveal that the PINK1-MIC60 pathway maintains remodeling of crista junctions, the complex I activity, and DA neuronal survival *in vivo*.

RESULTS

Inside Mitochondria, PINK1 Is Required for Maintenance of Crista Junctions

We determined whether PINK1 is present inside the mitochondria of *Drosophila*. By immuno-gold staining under transmission electron microscopy (TEM), we found that transgenic PINK1-Flag was evenly distributed inside the mitochondria, likely in the matrix or intermembrane space, as well as outside the mitochondria in the cytosol (Figure S1A). Human PINK1 transgene was used here and throughout the paper, owing to the functional conservation between human and fly PINK1 (Clark et al., 2006). Using proteinase K assays (Morais et al., 2014), we found that a fraction of endogenous *Drosophila* PINK1 (dPINK1) was present inside the mitochondria at the steady state (Figure S1B). We next examined mitochondrial crista structure under TEM and identified crista phenotypes in body wall muscles of *PINK1*-null late third instar larvae 120 hr after egg laying (AEL). Approximately 34.45% of total mitochondria appeared like an "onion" with concentric multi-layered and heavily packed crista membranes, and 58.13% were filled with small "vacuole"-like crista membranes. In both cases, crista junctions were significantly reduced. In *PINK1*-null mitochondria, there were only 1.03 ± 0.29 crista junctions/μm of mitochondrial circumference, whereas in wild-type mitochondria, there were 5.08 ± 0.32 crista junctions/μm (Figures 1B–1D). These results indicate that PINK1 is required for maintenance of crista junctions in late third instar larval body wall muscles. The mitochondrial shape became round in *PINK1*-null larvae, although the mitochondrial size was not significantly altered (Figure S1C). No pronounced muscle degeneration was observed in *PINK1*-null larvae (Figure S1D). We found the same onion- and vacuole-like mitochondria in larval body wall muscles using another independent *PINK1*-null allele (Figure S1E). In the nervous system, the phenotype of the onion-like cristae and loss of crista junctions existed only in the neuropils (enriched with synapses, dendrites, and axons) at the ventral nerve cords (VNCs), but not in the cell bodies at the VNC, in the segmental nerves (axons), or at the neuromuscular junctions (NMJs) in *PINK1*-null larvae (Figure S2). We then considered the possibility that mitochondrial cristae undergo PINK1-dependent remodeling when mitochondria move from the cell bodies into the neuropils. To explore this possibility, we measured the mitochondrial crista density (the number of cristae/mitochondrial area) and found that mitochondria in neuropils contained significantly more dense cristae with increased crista junctions than those in neuronal cell bodies, axons, or NMJs (Figure S3A), indicating that mitochondrial remodeling of crista structure occurs when mitochondria move into the neuropils from the cell body and mitochondrial respiratory activity increases (Hackenbrock, 1966; John et al., 2005). In addition, neuropils had more mitochondria (the volume mitochondria occupy/total volume) than neuronal cell bodies, axons, or NMJs (Figure S3B), suggesting that synapse and dendrite-enriched neuropils consume more energy (Lajtha et al., 2007). Therefore, when mitochondria move to subcellular compartments that may have elevated energy demands, they condense their cristae and increase crista junctions in third instar larvae. This structural plasticity requires PINK1, because in those regions of *PINK1*-null larvae mitochondrial cristae fail to remodel as in wild-type, and instead they display the onion-like membranes with loss of crista junctions (Figures 1, S1, and S2). Taken together, PINK1 is essential for mitochondria to increase crista junctions in selective subcellular areas in third instar larvae (Figure 1E).

We next determined the extent to which the physical presence of PINK1 inside the healthy mitochondria is required for maintenance of crista junctions. To do this, we ubiquitously expressed full-length PINK1, or PINK1$^{\Delta MTS}$ without the mitochondrial targeting sequence (MTS) that leads PINK1 import into mitochondria (Weihofen et al., 2009), in *PINK1*-null larvae. Both PINK1 transgenes were inserted in the same genomic site using the PhiC31 integrase-mediated transgenesis systems to ensure the same genomic regulations (Markstein et al., 2008), and their protein expression levels were comparable (Figure S4A). The aberrant crista structure and loss of crista junctions in *PINK1*-null flies were fully rescued by expressing full-length PINK1, but not by PINK1$^{\Delta MTS}$, in late third instar larval body wall muscles (Figures 1B–1D). Therefore, the import of PINK1 into healthy mitochondria is required for maintenance of crista junctions in larval muscles.

The onion- and vacuole-like mitochondria found in *PINK1*-null larvae differed from the previously reported "vacuolated (empty)" mitochondria with crista fragmentation in thoracic indirect flight muscles of *PINK1*-null adults (Clark et al., 2006; Park et al., 2006). We also observed the predominant vacuolated mitochondria in *PINK1*-null adults but did detect about 25% of the onion-like mitochondria at an earlier adult stage (day 3), which all converted to vacuolated mitochondria at day 5 (Figure S4B). This result suggests that the onion-like mitochondria may represent an earlier stage of mitochondrial pathology in adults. Expression of PINK1$^{\Delta MTS}$ failed to rescue the mitochondrial phenotypes and muscle degeneration in *PINK1*-null adult flies (Figures S4B and S4C), demonstrating the importance of PINK1 inside healthy mitochondria for adults as well.

It has been reported that *Parkin*-null adult flies exhibit similar vacuolated mitochondria as *PINK1*-null adults (Greene et al., 2003; Pesah et al., 2004). To answer the question of whether

The scale bars represent 500 nm. *Parkin*^{null} (*Park*^{25}); *Parkin*^{RV} (*Park*^{rva}); *PINK1*^{nul} (*PINK1*^{5}/*Y*; *da-GAL4*); *PINK1*^{null},*da* > *PINK1*$^{WT/\Delta MTS}$ (*PINK1*^{5}/*Y*;*UAS-hPINK1*$^{WT/\Delta MTS}$*-Flag*;*da-GAL4*); wild-type (*PE704/Y*, precise excision control males for *PINK1*^{5}/*Y*); WT, wild-type. Genotypes are written in the same way here and for all figures except otherwise stated. Comparisons with "wild-type" are shown. *p < 0.05, **p < 0.01, ***p < 0.001, and the box-whisker plots are used for all figures unless otherwise stated. See also Figures S1, S2, S3, and S4.

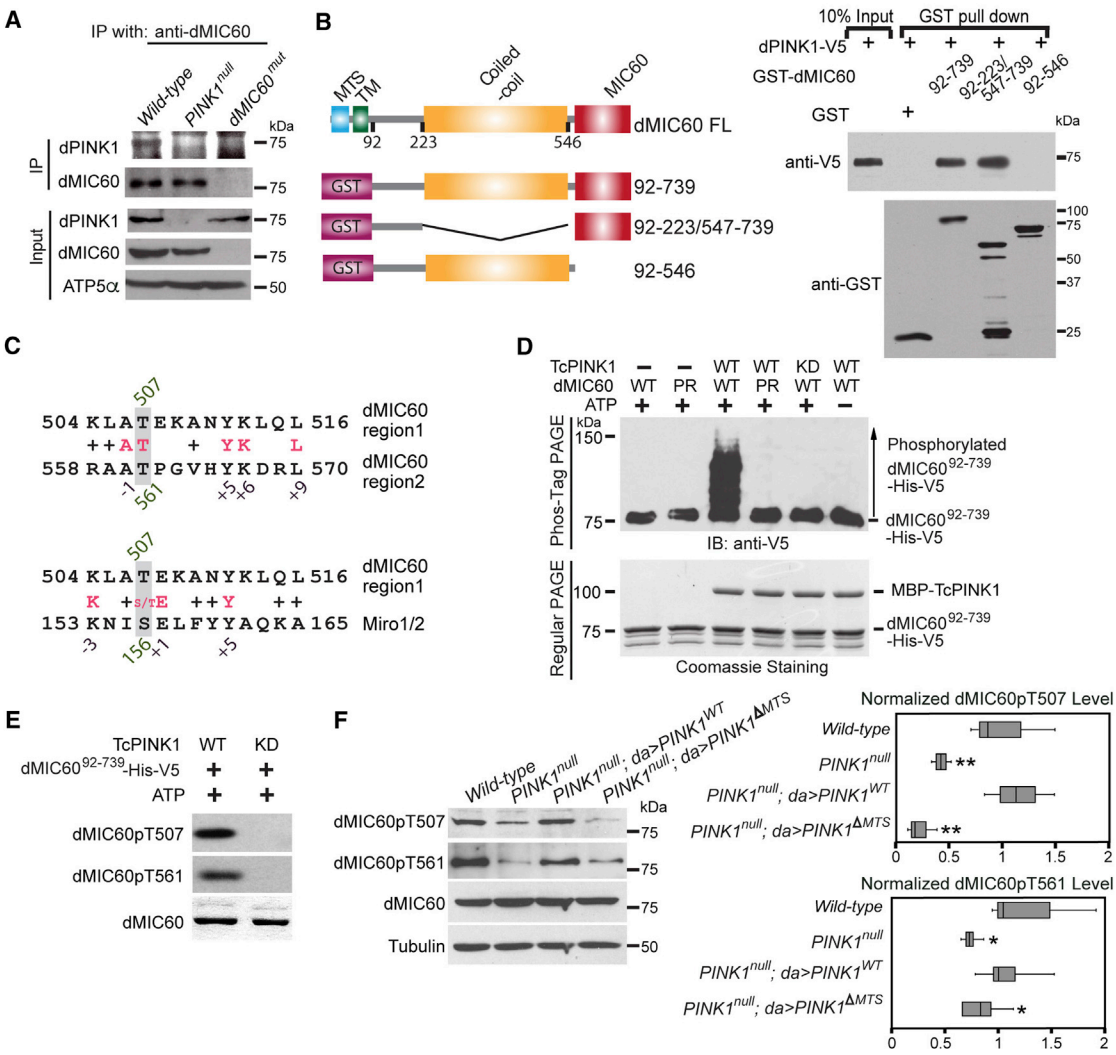

Figure 2. PINK1 Interacts with and Phosphorylates dMIC60

(A) Immunoprecipitations with anti-dMIC60 were performed using the mitochondrial fractions of pupae 72 hr after pupa formation (AFP).

(B) Schematic representation of the truncated GST-dMIC60 used in the *in vitro* co-precipitation. FL, full length. Samples were immunoblotted as indicated.

(C) Sequence alignments between the flanking regions of the two threonine sites in dMIC60 or between the phospho-peptides of dMIC60 and human Miro1/2.

(D) The upper blot is the phos-tag gel immunoblotted with anti-V5. The lower blot is the Coomassie-stained gel revealing the proteins in the reactions.

(E) The *in vitro* phosphorylation reactions were immunoblotted as indicated.

(F) Lysates of adults 5 days after eclosion were immunoblotted as indicated, and the band intensities of phospho-dMIC60 are normalized to those of total dMIC60. n = 3–6 independent experiments. Comparisons with wild-type are shown.

See also Figure S5.

Parkin-null larvae also show the onion- and vacuole-like mitochondria in their muscles as observed in *PINK1*-null larvae, we performed TEM on *Parkin*-null third instar larval body wall muscles. Surprisingly, about half of total mitochondria were normal (40.07%), and the majority of abnormal mitochondria (38.44%) displayed a "dumbbell" shape, in which two ends of one mitochondrion stretch extensively in the opposite directions while the OMM and crista junctions are intact (Figure 1F), implying a failure in fission. Thus, *PINK1* and *Parkin* mutant larvae show distinct phenotypes in crista structure. Collectively, our results reveal a novel function for PINK1 inside healthy mitochondria to regulate structural plasticity of mitochondrial crista junctions.

PINK1 Phosphorylates MIC60

We sought the mechanism by which PINK1 maintains crista junctions. A previous study has reported human MIC60 in a mass spectrometry screen searching for PINK1's binding partners (Weihofen et al., 2009). Interestingly, MIC60 has been demonstrated to play a crucial role in crista junction formation (John et al., 2005; Rabl et al., 2009). In flies, we found that endogenous dPINK1 physically interacted with endogenous *Drosophila* MIC60 (dMIC60) *in vivo* (Figure 2A), which was detected by a polyclonal antibody against dMIC60 protein (anti-dMIC60) generated by us. A band of the predicted size of dMIC60 protein was recognized by anti-dMIC60 in wild-type,

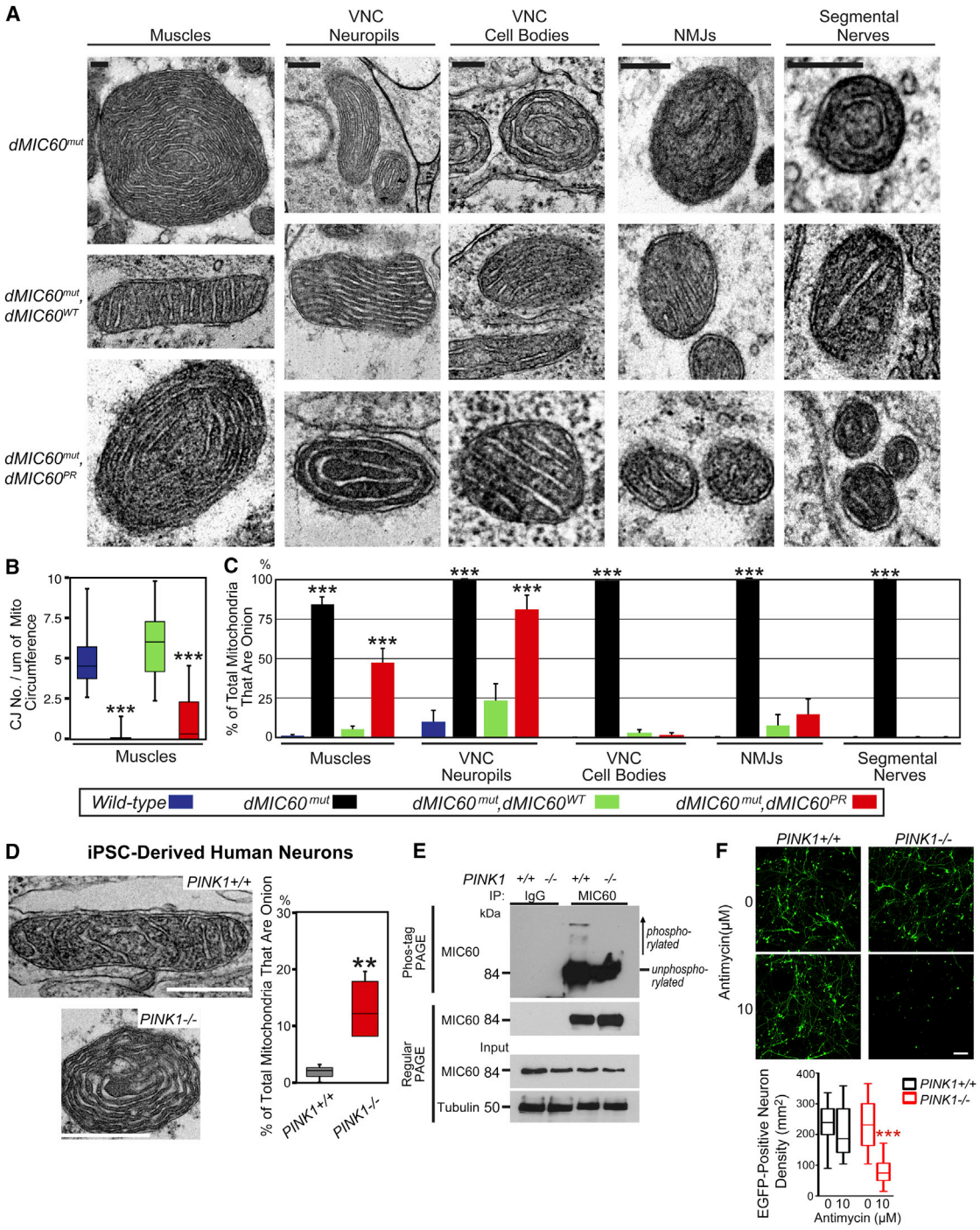

Figure 3. PINK1-Mediated Phosphorylation of dMIC60 Maintains Crista Junctions

(A) TEM images of body wall muscles, VNC, NMJs, or segmental nerves of late third instar larvae (120 hr AEL).

(B) Quantification of the number of crista junctions normalized to the length of the mitochondrial circumference. n = 30 mitochondria from 30 images obtained from 4–6 flies.

(C) Quantification of the percentage of total mitochondria per image. n = 17–236 mitochondria from 8–15 images from 4–6 larvae. Bar graphs and mean ± SEM are shown.

For (A)–(C), *dMIC60*^{mut} (*Tubulin-GAL4_dMIC60*$^{LL02849/LL02849}$); *dMIC60*^{mut},*dMIC60*$^{WT/PR}$ (*UAS-dMIC60*$^{WT/PR}$-Myc;*Tubulin-GAL4_dMIC60*$^{LL02849/LL02849}$); wild-type (*w*^{1118}). Comparisons with wild-type are shown.

(D) TEM images of iPSC-derived neurons. n = 172–198 mitochondria from 30 images from 3 independent experiments.

(legend continued on next page)

but not in a *dMIC60* mutant (*dMIC60*^{mut}) (described later), confirming the specificity of this antibody (Figure 2A). We determined that dPINK1 and dMIC60 also interacted *in vitro* and mapped the region of dMIC60 required for binding to dPINK1 (Figure 2B). We bacterially expressed N-terminal glutathione S-transferase (GST)-tagged dMIC60 with different truncations: GST-dMIC60$^{92–739}$ (lacking the N-terminal MTS and transmembrane [TM] domains); GST-dMIC60$^{92–223_547–739}$ (lacking the N-terminal MTS and TM and the coiled-coil domains); or GST-dMIC60$^{92–546}$ (lacking the N-terminal MTS and TM and the C-terminal domains; Körner et al., 2012) and incubated it with glutathione Sepharose beads before incubation with bacterially purified C-terminal V5-tagged dPINK1. We found that dPINK1 co-precipitated with GST-dMIC60$^{92–739}$ and GST-dMIC60$^{92–223_547–739}$, but not with GST-dMIC60$^{92–546}$ (Figure 2B), suggesting that the C-terminal amino acids (aas) 547-739 of dMIC60 are required for directly binding to dPINK1.

Because PINK1 is a Ser/Thr kinase, we next determined whether dMIC60 is a substrate of PINK1. To do this, we performed an *in vitro* PINK1 kinase assay on bacterially expressed dMIC60. dMIC60$^{92–739}$ was incubated with either purified *Tribolium castaneum* PINK1 (TcPINK1)—the known form of PINK1 that remains active *in vitro* (Woodroof et al., 2011)—or inactive kinase-dead TcPINK1 (TcPINK1KD) prior to mass spectrometric and phos-tag acrylamide analysis. Using mass spectrometry, we identified two dMIC60 sites, threonine 507 and 561, which were phosphorylated; these two sites were not phosphorylated in the other negative controls, although the unphosphorylated peptides were detected with the same efficiency among all reactions (Figures 2C, 2D, and S5). In the mass spectrometric analysis, we encompassed approximately 90% of the total residues of dMIC60$^{92–739}$. Using phos-tag acrylamide, where phosphorylated proteins migrate slower because of binding to the phos-tag ligands, we detected phosphorylated dMIC60 only in the reaction with ATP and TcPINK1 both present, but not when ATP or TcPINK1 was absent (Figure 2D). When both the two phosphorylation sites were mutated to phosphorylation-resistant (PR) alanine, dMIC60 was no longer phosphorylated by TcPINK1 (Figure 2D), which indicates that these two sites are the main phosphorylation residues. We generated two antibodies against phosphorylated dMIC60 at threonine 507 and 561, respectively, and found that the band intensities recognized by anti-phospho-dMIC60 were completely abolished by kinase-dead TcPINK1KD *in vitro* (Figure 2E), confirming the specificity of these antibodies. Phosphorylation at both sites was significantly reduced in *PINK1*-null flies and required the physical presence of PINK1 inside the mitochondria (Figure 2F). Taken together, PINK1 phosphorylates dMIC60 both *in vivo* and *in vitro*.

PINK1-Mediated Phosphorylation of dMIC60 Maintains Crista Junctions in *Drosophila*

Our finding that the IMM protein dMIC60 is a substrate of PINK1 (Figure 2) suggests the intriguing possibility that PINK1 might maintain crista junctions by phosphorylating dMIC60. If this hypothesis were true, blocking phosphorylation of dMIC60 by mutating the phosphorylation sites (Figure 2) might cause similar crista phenotypes as removing PINK1. To test this hypothesis directly, we ubiquitously expressed wild-type dMIC60-upstream activating sequence (UAS)-dMIC60^{WT}- or UAS-dMIC60^{PR} (Figure 2) in a *dMIC60* mutant background (*dMIC60*^{mut}) (Tsai et al., 2017) without the expression of endogenous *dMIC60* (Figures 2A, S6A, and S6B). This allele of *dMIC60* is pupal lethal (Tsai et al., 2017) and caused loss of crista junctions ubiquitously in late third instar larvae (Figures 3A–3C). Both the wild-type and mutant dMIC60 transgenes were inserted in the same genomic location (Markstein et al., 2008), and their expression levels in *dMIC60*^{mut} were comparable (Figure S6B). Ubiquitous expression of either transgene in *dMIC60*^{mut} flies did not exceed the endogenous dMIC60 level (Figure S6B) and thus circumvented the potential adverse effect by overexpression. dMIC60^{WT} in *dMIC60*^{mut} larvae completely restored their crista structure (Figures 3A–3C). In contrast, dMIC60^{PR} in *dMIC60*^{mut} failed to restore crista junctions in muscles and neuropils but could rescue crista phenotypes in neuronal cell bodies, axons, and NMJs in third instar larvae (Figures 3A–3C). Thus, dMIC60^{PR} in *dMIC60*^{mut} mirrors the crista phenotypes of *PINK1*-null flies: mitochondria lose their crista junctions in muscles and neuropils (Figures 1, 3, and S2). These results provide evidence that PINK1-mediated phosphorylation of dMIC60 is required for mitochondria to increase crista junctions in selective subcellular areas in *Drosophila*.

The PINK1-MIC60 Pathway Is Conserved in Humans

To determine whether the phosphorylation sites are conserved in humans, we knocked down endogenous human MIC60 by RNAi in HEK293T cells and expressed either RNAi-resistant wild-type or phospho-resistant human MIC60 with the two conserved sites (serine 518 and threonine 587) mutated to alanine (Figure S6C). We found that MIC60 RNAi knockdown in HEK293T cells resulted in the onion-like mitochondria with loss of crista junctions under TEM, which was fully rescued by the expression of MIC60^{WT}, but not by MIC60^{PR} (Figure S6D). We confirmed that expression of MIC60^{PR} led to loss of phosphorylation of MIC60 in those cells as detected by phos-tag gels (Figure S6E), suggesting that the two conserved sites are also the main phosphorylation residues in human MIC60. Notably, cells with MIC60^{PR} were significantly more vulnerable to oxidative stress induced by H_2O_2 treatment than cells with MIC60^{WT}, detected by the propidium iodide (PI) staining (Figure S6F). We also utilized induced pluripotent stem cell (iPSC)-derived human neurons with *PINK1* knockout and their isogenic wild-type controls. Under TEM, we detected about 15% of total neuronal mitochondria exhibiting the onion-like structure in *PINK1* loss-of-function neurons compared to only 2% in wild-type (Figure 3D). We confirmed that phosphorylation of endogenous

(E) Immunoprecipitates from iPSC-derived neurons as indicated were run in a phos-tag gel and immunoblotted with anti-MIC60. The lower blots are the regular PAGE showing immunoprecipitation (IP) and input.

(F) iPSC-derived neurons were transfected with EGFP and treated with antimycin A for 6 hr. The density of EGFP-positive neurons, which indicate live neurons, was calculated and compared to that without Antimycin A treatment. n = 30 imaging fields from 3 independent transfections.

The scale bars represent (A) 100 nm, (D) 500 nm, and (F) 100 μm. See also Figure S6.

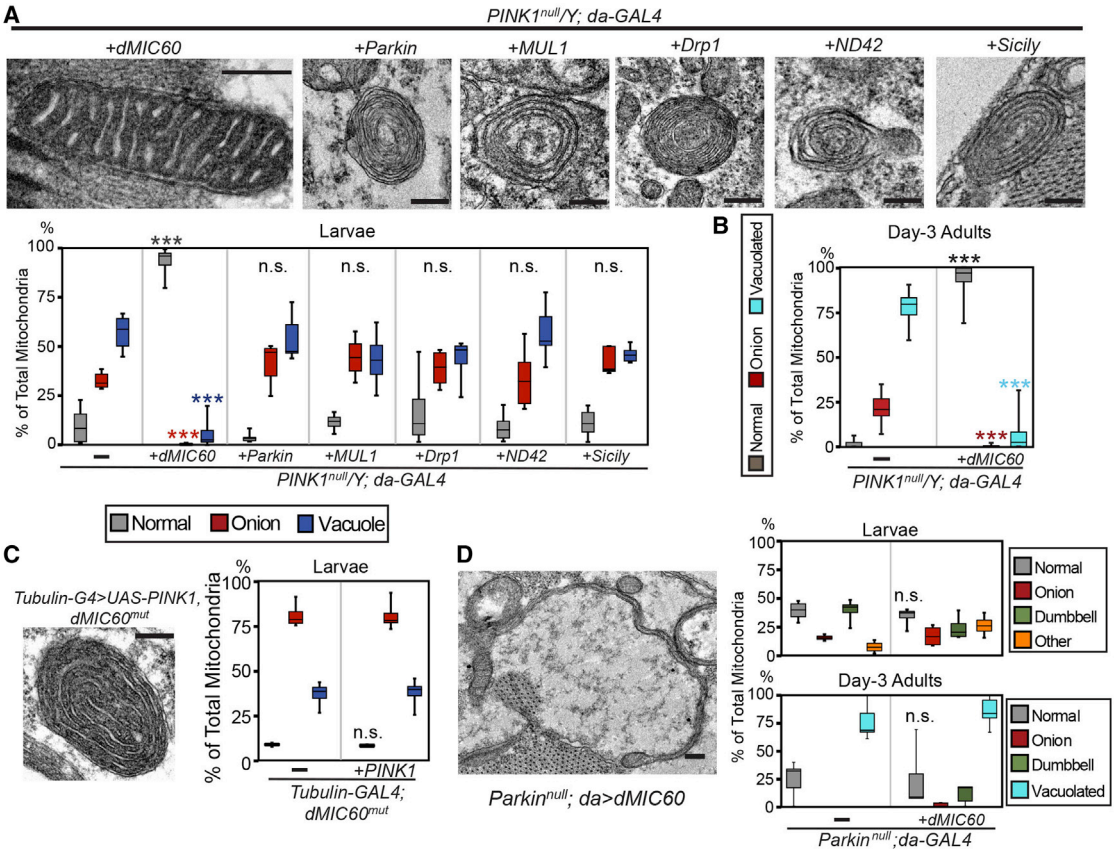

Figure 4. dMIC60 Restores Crista Structure of *PINK1*-Null

(A, C, and D) TEM images of body wall muscles of late third instar larvae (120 hr AEL) with the background of *PINK1* null (A), *dMIC60*^{mut} (C), or *Parkin* null (D). (A–D) Quantification of the percentage of total mitochondria per TEM image from body wall muscles of late third instar larvae or thoracic indirect flight muscles of 3-day-old adults with the background of *PINK1* null (A, larvae; B, adults), *dMIC60*^{mut} (C, larvae), or *Parkin* null (D, both). For larvae, n = 219–371 mitochondria from 27–32 images obtained from 4–6 flies. For adults, n = 106–331 mitochondria from 30–31 images obtained from 5 or 6 flies. Comparisons with the group to the left are shown. The scale bars represent 500 nm.

See also Figure S6.

human MIC60 was lost in *PINK1* knockout neurons using phos-tag gels (Figure 3E), verifying that PINK1 also mediates MIC60 phosphorylation in human neurons. Importantly, these *PINK1* loss-of-function neurons were more sensitive to oxidative stress triggered by antimycin A treatment (Figure 3F), similar to a key feature of PD patients-derived neurons (Hsieh et al., 2016). These results validate the PINK1-MIC60 pathway in human cells, including neurons, and its importance to crista junction formation and cellular survival.

dMIC60 Rescues the Defect in Crista Structure of *PINK1*-Null Flies

Because dMIC60 is a substrate of PINK1 for maintaining crista junctions (Figures 2 and 3), this places *dMIC60* genetically downstream of *PINK1*. To confirm their epistatic relationship, we ubiquitously expressed UAS-dMIC60 in a *PINK1*-null background or UAS-PINK1 in *dMIC60*^{mut}. Remarkably, upregulating dMIC60 completely rescued all the abnormal crista phenotypes in both *PINK1*-null larval and adult muscles (Figures 4A and 4B); on the contrary, PINK1 expression did not rescue the crista phenotypes in *dMIC60*^{mut} larval muscles (Figure 4C). Importantly, these results suggest that overexpression of dMIC60 that is not phosphorylated by PINK1 compensates for the lack of PINK1. Upregulation of dMIC60 in *Parkin*-null flies did not rescue their crista and behavioral phenotypes (Figures 4D and S6G). Thus, *dMIC60* functions downstream of *PINK1* to maintain crista structure in muscles.

A few other factors have also been reported as being downstream of PINK1 at the adult stage, such as Parkin (Clark et al., 2006; Park et al., 2006), the complex I (Morais et al., 2014; Pogson et al., 2014), the mitochondrial fission-fusion machinery (Poole et al., 2010; Yang et al., 2008; Ziviani et al., 2010), and MUL1 (Yun et al., 2014). To determine whether these known PINK1-dependent pathways interplay with the PINK1-MIC60 pathway for crista structure maintenance in larval muscles, we expressed UAS-Parkin (a ubiquitin E3 ligase), UAS-ND42 (a complex I subunit), UAS-Sicily (co-chaperone of ND42), UAS-Drp1 (controls mitochondrial fission), or UAS-MUL1 (a ubiquitin E3 ligase) in *PINK1*-null larvae. All five transgenes have been shown to rescue the mitochondrial morphological phenotypes

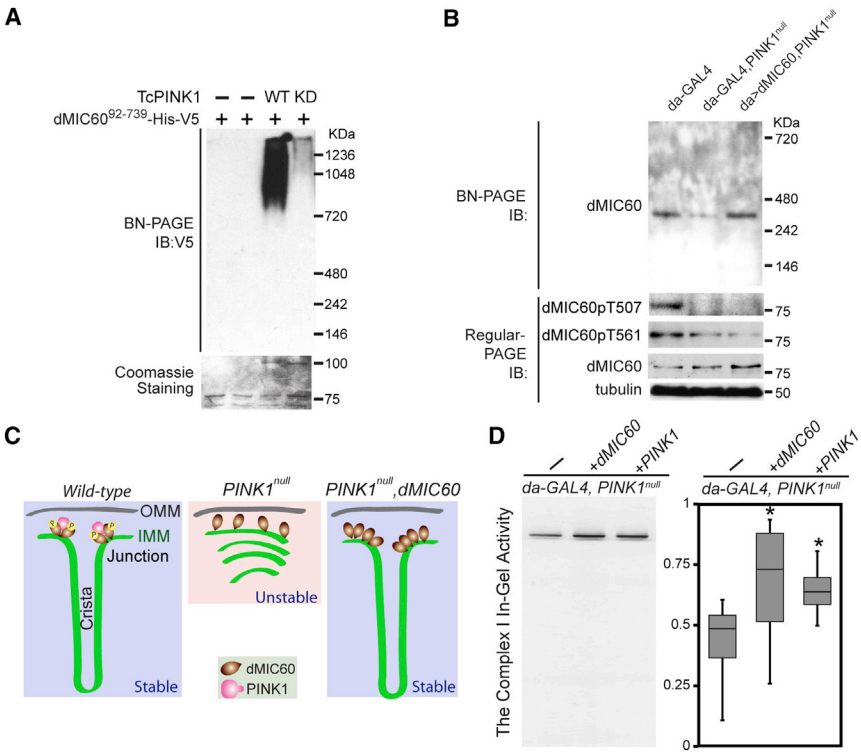

Figure 5. Both Phosphorylation and Overexpression of dMIC60 Stabilize dMIC60 Oligomerization

(A) BN-PAGE was immunoblotted with anti-V5. Note that the shifted bands may not represent the physiological forms of oligomers due to the large amount of proteins present *in vitro*.

(B) dMIC60 or phosphorylated dMIC60 was immunodetected in whole-body lysates of 5-day-old adults as indicated, using either BN-PAGE or regular-PAGE. dMIC60 migrates as a tetramer or oligomerizes with other proteins based on the size in BN-PAGE. The same results were observed for 3 times.

(C) Schematic representation of the potential impact of PINK1-mediated phosphorylation or overexpression of dMIC60 on dMIC60 oligomerization and crista curvatures.

(D) The in-gel activity of complex I was measured. The representative native gel and quantification of the band intensities compared to "*PINK1*^{null}, *da-GAL4*" are shown. n = 100 adults 5 days after eclosion for each experiment and total 4 independent experiments.

in *PINK1*-null adult muscles to varying degrees. In striking contrast to *dMIC60*, none of them rescued the onion- or vacuole-like mitochondria in *PINK1*-null larval muscles (Figure 4A). These results indicate *dMIC60* as the strongest downstream factor of *PINK1* in larvae to maintain crista structure.

Both Phosphorylation and Upregulation of dMIC60 Promote dMIC60 Oligomerization

Here, we have shown that both PINK1-mediated phosphorylation of dMIC60 (Figures 1, 2, and 3) and overexpression of dMIC60 that is not phosphorylated by PINK1 (Figures 4A and 4B) maintain crista junctions. These results suggest that upregulated and phosphorylated dMIC60 cause the same functional impact on crista junctions. Because homo-oligomerization of MIC60 has been shown to be crucial for the formation of crista junctions (John et al., 2005; Mun et al., 2010), we then reasoned that upregulated and phosphorylated dMIC60 both promote dMIC60 oligomerization. We immunoblotted dMIC60 using blue-native (BN) SDS-PAGE to detect dMIC60 oligomerization. Phosphorylation of dMIC60 by wild-type TcPINK1 *in vitro* caused retardation of dMIC60 migration above 720 kDa, indicative of dMIC60 oligomers, and this oligomerization was abolished by kinase-dead TcPINK1KD (Figure 5A). This reveals that PINK1-mediated phosphorylation of dMIC60 promotes dMIC60 oligomerization *in vitro*. To detect the dMIC60 complex *in vivo*, we immunoblotted dMIC60 from fly lysates. We found that, in wild-type background, dMIC60 migrated as an oligomer (Mun et al., 2010; Figure 5B). dMIC60 oligomerization was significantly inhibited in *PINK1*-null (Figure 5B), indicating that PINK1-mediated phosphorylation of dMIC60 promotes dMIC60 oligomerization *in vivo*. Overexpressed dMIC60 in *PINK1*-null fully restored its oligomerization (Figure 5B), mimicking the effect of phosphorylated dMIC60 on the dMIC60 complex. Importantly, overexpression of dMIC60 in *PINK1*-null did not cause more phosphorylation at either threonine 507 or 561 than that in *PINK1*-null alone without dMIC60 overexpression (Figure 5B), excluding the possibility that the restoration of oligomerization is caused by increased phosphorylation by a kinase other than PINK1. Therefore, both upregulation and phosphorylation of dMIC60 stabilize dMIC60 oligomerization, yielding the same favorable functional effect for crista junctions (Figure 5C).

dMIC60 Rescues Diverse Organelle and Organismal Phenotypes of *PINK1*-Null Flies

Aberrant crista structure may compromise mitochondrial health and accumulate oxidative stress, leading to detrimental cellular and organismal consequences. Indeed, *PINK1*-null flies display numerous defects in the complex I activity, ATP level, $\Delta\Psi$m, locomotor, and DA neuronal survival (Clark et al., 2006; Morais et al., 2014; Park et al., 2006; Pogson et al., 2014; Tsai et al., 2014). We determined whether an impaired mitochondrial crista structure underlies these dysfunctions. We ubiquitously expressed UAS-dMIC60 in *PINK1*-null flies to restore their crista structure (Figures 4A and 4B) and determined whether this could alleviate these phenotypes. We found that dMIC60 completely rescued *PINK1*-null's defects in the complex I activity (Figure 5D), ATP level (Figure 6A), $\Delta\Psi$m detected by tetramethylrhodamine (TMRM) in larval muscles (Figure 6B), and larval crawling ability (Figure 6C). On the contrary, expression of Parkin, ND42, or Drp1, which fails to rescue the crista phenotypes in *PINK1*-null larvae (Figure 4A), did not fully rescue their crawling deficit (Figure 6C). Additionally, upregulating dMIC60 in *PINK1*-null flies

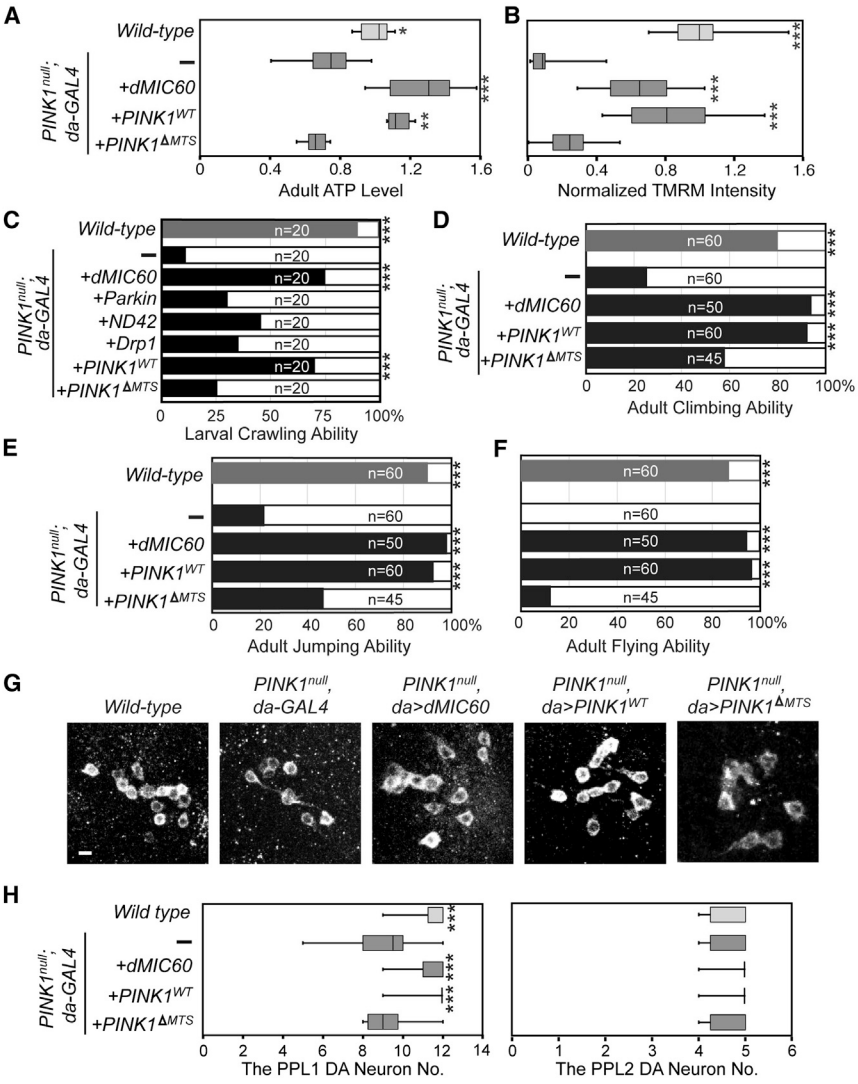

Figure 6. dMIC60 Rescues Various Phenotypes of *PINK1*-Null

(A) Quantification of the total ATP level in adult flies 5 days after eclosion. n = 5 adults for each experiment and total 6 independent experiments.

(B) Quantification of the mitochondrial/cytoplasmic TMRM fluorescent intensity in body wall muscles of third instar larvae. n = 6 larvae.

(C–F) The crawling ability of third instar larvae (C) and the climbing (D), jumping (E), and flying (F) abilities of adult flies 5 days after eclosion were quantified. n = 20–60 flies. The percentage of flies that are scored as a "1" (able to do it) is shown in black/gray bars, and the percentage of flies that are scored as a "0" (unable to do it) is shown in white bars. The chi-square test is used as the data are categorical.

For (A)–(F), wild-type, *PE704/Y*.

(G) The PPL1 clusters of DA neurons visualized by anti-TH in adult brains 15 days after eclosion. $PINK1^{null}$, $PINK1^{B9}/Y$; wild-type, $PINK1^{RV}/Y$ (precise excision control males for $PINK1^{B9}/Y$). $PINK1^{B9}/Y$ exhibits the same crista impairments as $PINK1^{5}/Y$ used in the other figures (Figure S1E).

(H) Quantification of the DA neuron number in one PPL1 or one PPL2 cluster per brain of adult flies 15 days after eclosion. n = 10–14 brains. Genotypes are the same as in (G). For all panels, comparisons with $PINK1^{null}$, *da-GAL4* are shown. The scale bar represents 5 μm.

completely rescued their climbing, jumping, and flying defects 5 days after eclosion and DA neurodegeneration in the protocerebral posterior lateral 1 (PPL1) cluster 15 days after eclosion (Figures 6D–6H). Importantly, expression of the non-mitochondrial-targeting mutant $PINK1^{\Delta MTS}$ (Weihofen et al., 2009), which does not restore the crista structure in *PINK1*-null flies (Figures 1 and S4), did not rescue their impairments in the $\Delta\Psi m$, ATP level, behavior, and DA neuronal number (Figure 6). In summary, *dMIC60* functions downstream of *PINK1* to maintain mitochondrial functions and locomotion and to prevent DA neurodegeneration. In a broader sense, this discovery adds a new player, MIC60, to a cellular pathway with a key role in PD.

Rare Coding Variants in the MTS of *MIC60* Found in PD Patients Are Damaging in Flies

Recessive loss-of-function *PINK1* mutations are a well-established cause of familial forms of early-onset PD (Valente et al., 2004). Our discovery of a new PINK1-MIC60 pathway crucial for mitochondrial functions and neuronal integrity suggests the possibility for *MIC60* coding mutations in PD. We first sequenced the entire coding region of *MIC60* gene (*IMMT*: 2p11.2, OMIM*600378; Table S1) in 100 familial PD probands, 250 apparently sporadic early-onset PD patients, and 350 age/gender/ethnicity-matched controls of East Asian origin, recruited from National Taiwan University Hospital. We identified one heterozygous missense mutation in *MIC60*, c.G50T (p.C17F), in 1 familial dominant patient (Figures S7A and S7B) but no variants in controls. We genotyped this variant in additional 602 independent sporadic late-onset patients and 581 age/gender/ethnicity-matched control subjects of East Asian origin. We detected the heterozygous p.C17F mutation in 1 sporadic patient (Figures S7C and S7D), but not in controls. The p.C17F variant is located in the MTS region of MIC60. Interestingly, recent studies have suggested that rare MTS variants in the PD-linked gene *CHCHD2* play a role in the risk of PD (Ogaki et al., 2015). We sequenced the MTS region in additional 859 Caucasian PD patients and 871 control individuals recruited at Mayo Clinic, USA. We identified two heterozygous MTS missense mutations (p.A4V and p.R25H) in 2 sporadic PD patients and one heterozygous MTS missense mutation (p.R31C) in 2 control individuals (Figure 7A; Table S2). We next analyzed the exome sequencing data released by Parkinson's Progression Markers Initiative (PPMI) (http://www.ppmi-info.org). This study includes 422 recently diagnosed PD patients and 163 healthy controls of Caucasian origin, recruited from

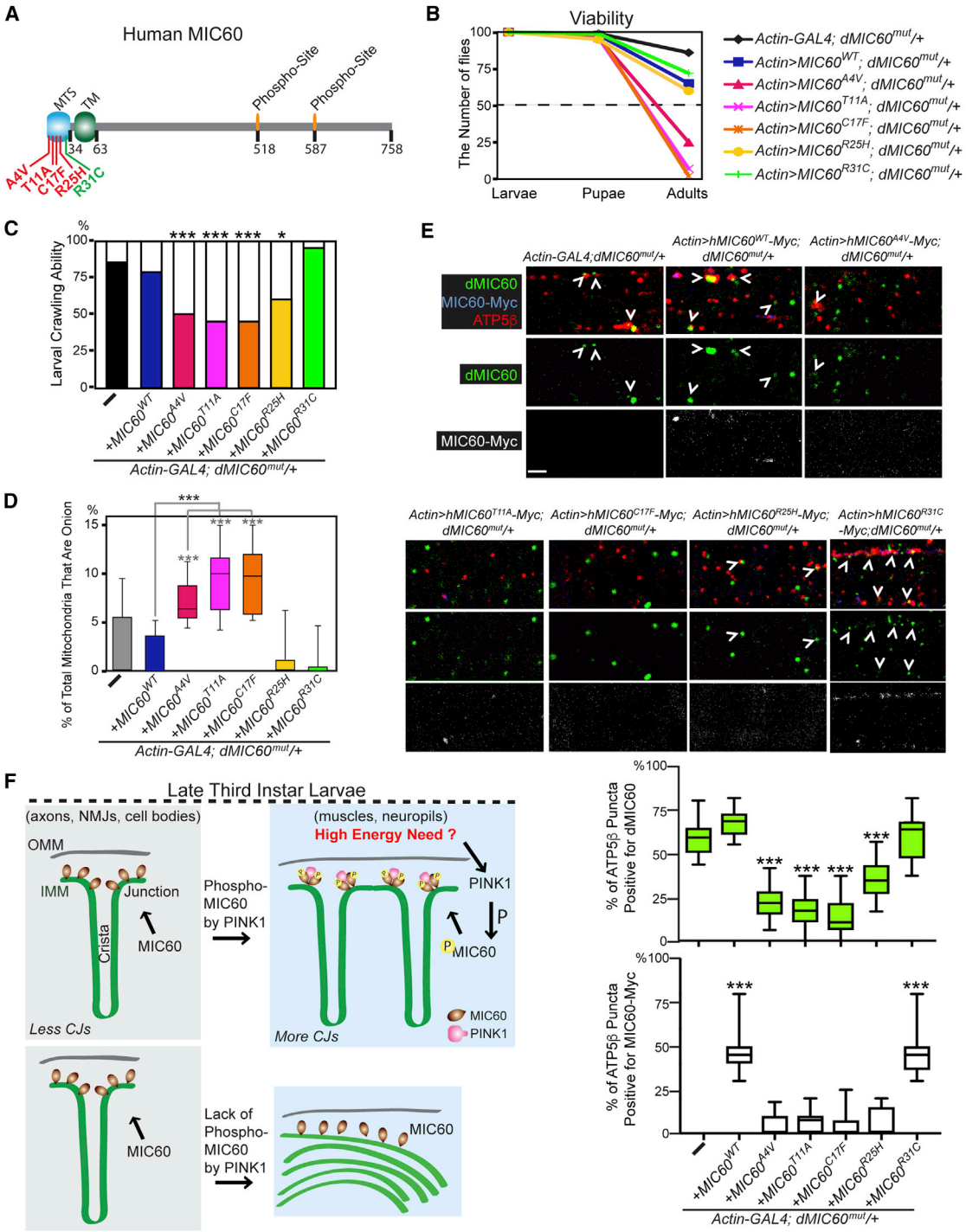

Figure 7. *MIC60* Variants in Humans and *Drosophila*

(A) Depiction of the *MIC60* MTS variants identified in this study.

(B) Viability analysis. One hundred late third instar larvae of each genotype were collected, and the numbers of their pupae and adults were subsequently counted.

(C) The crawling ability of third instar larvae with genotypes as indicated. n = 20 larvae. The percentage of flies that are scored as a "1" is shown in black/color bars, and the percentage of flies that are scored as a "0" is shown in white bars. The chi-square test is used.

(D) Quantifications of mitochondria in TEM images from body wall muscles of late third instar larvae (120 hr AEL; representative images in Figure S7F). n = 20 images from 6 flies.

(E) Single sections of confocal images showing immunostaining against endogenous dMIC60 (green) or exogenously expressed human MIC60-Myc (blue/white) in body wall muscles of third instar larvae. Red is the mitochondrial marker ATP5β. Note that anti-dMIC60 does not recognize expressed human MIC60. White

(legend continued on next page)

the United States and Europe. We again identified one heterozygous MTS mutation (p.T11A) in 1 sporadic PD patient (Figure 7A), which was not present in any SNP database (Table S2). As all variants identified so far are rare (minor allele frequency < 0.5%; Table S2), we compared the cumulative allele frequency of MTS coding variants in PD patients with that in the respective ethnic groups in the genome Aggregation Database (gnomAD) (http://gnomad.broadinstitute.org), the largest internationally combined database aggregating population variant frequencies, and combined the results using meta-analysis. We found that the occurrence of MTS coding variants was significantly higher in PD patients than that in gnomAD (meta odds ratio [OR] = 3.610; meta p = 0.023; Table S2).

We conducted an unbiased screen in flies to determine the functional pathogenicity of those *MIC60* MTS mutations. Because all the identified variants are heterozygous, we ubiquitously expressed the human MIC60 transgenes in a heterozygous *dMIC60*^{mut} background (*dMIC60*^{mut}/+). All the wild-type and mutant human *MIC60* transgenes were inserted in the same genomic location (Markstein et al., 2008) and expressed at similar levels (Figure S7E). Strikingly, expression of MIC60A4V, T11A, or C17F found in PD patients in "*dMIC60*^{mut}/+" flies, but not of wild-type MIC60 or R31C found in healthy controls, led to severe adult lethality and significantly impaired the larval crawling ability, although flies with the *dMIC60*^{mut}/+ background genotype were normal (Figures 7B and 7C). Expression of the R25H variant, found in one PD patient, compromised the larval crawling ability, but not viability (Figures 7B and 7C). Importantly, expression of MIC60A4V, T11A, or C17F in *dMIC60*^{mut}/+ impaired mitochondrial crista junction formation causing the onion-like mitochondria in late third instar larval body wall muscles (Figures 7D and S7F). Because these mutations reside in the MTS, we reasoned that they may disrupt the mitochondrial targeting ability of MIC60. To test this hypothesis, we immunostained endogenous fly dMIC60, exogenously expressed human MIC60 by the Myc tag, and the subunit of the mitochondrial ATP synthase ATP5β as a mitochondrial marker in muscles (Morais et al., 2014). We verified the specificity of the immunostaining signals of both anti-dMIC60 and anti-Myc: the anti-dMIC60 signals disappeared in *dMIC60*^{mut} flies (Figure S7G) and the anti-Myc signals were undetectable in non-transgenic flies (Figure 7E). We observed that wild-type human MIC60 or MIC60R31C found in healthy controls largely localized to mitochondria, whereas MIC60A4V, T11A, C17F, or R25H found in patients exhibited a non-mitochondrial diffuse pattern (Figure 7E), suggesting that patients-linked variants disrupt the mitochondrial localization of MIC60. Interestingly, endogenous dMIC60 significantly localized to mitochondria in *dMIC60*^{mut}/+ flies or when exogenous wild-type human MIC60 or MIC60R31C was present, but this mitochondrial localization was greatly reduced when human MIC60A4V, T11A, C17F, or R25H was expressed (Figure 7E). These results demonstrate that *MIC60* MTS variants found in PD patients damage the mitochondrial-targeting ability of MIC60 in a dominant-negative way in *Drosophila*. Our novel strategies combining human genetics and functional screen focused on a defined coding region thus identify *MIC60* variants that are highly damaging *in vivo*.

DISCUSSION

In the present study, we have determined that the PD-causing kinase PINK1 phosphorylates MIC60 to maintain crista junctions in *Drosophila* and in human neurons. This mechanism represents a novel form of PINK1-mediated phosphorylation, as PINK1 is well-known to mediate mitophagy by phosphorylating its substrates on the surface of unhealthy mitochondria, dependent on the ΔΨm. In this new mechanism, PINK1-mediated phosphorylation of MIC60 is dependent on the physical presence of PINK1 inside healthy mitochondria and is likely activated by elevation of cellular energy demands (Figure 7F).

We have shown that overexpressed dMIC60 is able to compensate for the loss of phosphorylation by PINK1 in *Drosophila* (Figures 4, 5, and 6). This bears a resemblance to the regulation of Parkin or ND42, which has been reported to be phosphorylated by PINK1 directly or indirectly (Kazlauskaite et al., 2014; Kondapalli et al., 2012; Morais et al., 2014). Overexpression of wild-type Parkin or ND42 rescues some of the *PINK1*-null's phenotypes (Clark et al., 2006; Park et al., 2006; Pogson et al., 2014), although how this is achieved by unphosphorylated Parkin or ND42 remains unclear. Here, we have revealed that overexpressed dMIC60 mimics phosphorylated dMIC60 to stabilize MIC60 oligomerization (Figure 5), which is essential for crista junction formation (John et al., 2005; Mun et al., 2010). When phosphorylation of MIC60 is absent in *PINK1*-null, overexpressed MIC60 can stabilize its own oligomerization (Figure 5). Future structural work could help define the impact of PINK1-mediated phosphorylation on the stoichiometry of the MIC60 complex.

The onion-like mitochondria with loss of crista junctions are a well-established feature of impairments in the MICOS complex (von der Malsburg et al., 2011). This unique aberration in crista membrane topology disrupts complex assembly and solute gradients, both required for mitochondria oxidative phosphorylation (Mannella et al., 2013), and consequently leads to severe defects at the cellular and organismal levels (John et al., 2005; Mun et al., 2010; von der Malsburg et al., 2011). Our findings extend this mitochondrial phenomenon to the PD-causing gene PINK1. Future work is warranted to determine whether this mitochondrial phenotype exists in PD patients and whether it contributes to PD pathogenesis. Plasticity of crista structure must be seamlessly tailored to shifts in energy needs in highly energetic neurons to allow for vigorous alterations in their activities and circuitry. Our work thus implicates the vital importance of mitochondrial crista structure and its ability to remodel for dynamically balancing the metabolic homeostasis of a cell.

arrow heads show colocalization between endogenous dMIC60 and ATP5β. The scale bar represents 5 μm. Quantification of the percentage of ATP5β puncta that are also positive for dMIC60 or MIC60-Myc is shown. n = 12 images from 4–6 larvae.

(C–E) Comparisons with "*Actin-GAL4*;*dMIC60*^{mut}/+" are shown except indicated otherwise.

(F) Schematic representation of PINK1-dependent plasticity of crista junctions in third instar larvae.

See also Figure S7 and Tables S1 and S2.

STAR★METHODS

Detailed methods are provided in the online version of this paper and include the following:

- KEY RESOURCES TABLE
- CONTACT FOR REAGENTS AND RESOURCE SHARING
- EXPERIMENTAL MODEL AND SUBJECT DETAILS
  - Fly Stocks
  - Human Subjects
- METHOD DETAILS
  - Generation of dMIC60 Antibodies
  - Constructs
  - Analysis of the ΔΨm Using TMRM
  - Detection of ATP Level
  - Immunocytochemistry and Confocal Microscopy
  - Mitochondrial Assays
  - Protein Biochemical Assays
  - TcPINK1 Kinase Assay
  - Mass Spectrometry
  - Transmission Electron Microscopy
  - Behavior Assay
  - Human Cell Experiments
- QUANTIFICATION AND STATISTICAL ANALYSES

SUPPLEMENTAL INFORMATION

Supplemental Information includes seven figures and two tables and can be found with this article online at https://doi.org/10.1016/j.molcel.2018.01.026.

ACKNOWLEDGMENTS

We thank Drs. B. Lu, J. Chung, M. Guo, S.K. Park, H. Bellen, L. Pallanck, and T. Clandinin for reagents and J. Perrino and the Stanford Cell Science Imaging EM Facility (1S10RR026780-01; the National Center for Research Resources) for assistance with the EM work. This work was supported by the Department of Defense (PR150380, X.W.; W81XWH-17-1-0249, O.A.R), the Alfred P. Sloan Foundation (X.W.), the Klingenstein Foundation (X.W.), the Shurl and Kay Curci Foundation (X.W.), the Marie Curie Career Integration Grant (D.W.), the Junior Group Leader Fellowship of the Bonfor-Program at the University Hospital Bonn (D.W.), the Graduate Research Fellowship Program of the National Science Foundation (A.P.), the Postdoctoral Research Abroad Program of the National Science Council, Taiwan (P.T.), the awards from Mayo Clinic Neuroscience Focused Research Team and Mayo Clinic Center for Regenerative Medicine (Z.K.W. and O.A.R.), the Michael J. Fox Foundation (O.A.R.), NIH/NINDS (R01 NS078086; O.A.R.), the gifts from Carl Edward Bolch Jr. and Susan Bass Bolch (Z.K.W.), the Sol Goldman Charitable Trust (Z.K.W.), and Donald G. and Jodi P. Heeringa (Z.K.W.). Mayo Clinic Florida is supported by a Morris K. Udall PD Research Center of Excellence (NINDS P50 no. NS072187). PPMI is funded by the Michael J. Fox Foundation for Parkinson's Research and funding partners, including Abbvie, Avid, Biogen, Bristol-Myers Squibb, Covance, GE Healthcare, Genentech, GlaxoSmithKline, Lilly, Lundbeck, Merck, Meso Scale Discovery, Pfizer, Piramal, Roche, Servier, and UCB.

AUTHOR CONTRIBUTIONS

P.-I.T., C.-H.H., A.M.P., and M.J.K. designed and performed the fly and cell experiments and made the figures. C.-H.L., R.-M.W., Z.K.W., and O.A.R. sequenced the patients. V.N., M.D.G., O.A.R., and J.C. analyzed the human genetics data. C.S. and D.W. performed mass spectrometry. X.W. conceived and supervised the project, designed the experiments, and wrote the paper with the assistance from all authors.

DECLARATION OF INTERESTS

The authors declare no competing interests.

Received: September 13, 2017
Revised: December 7, 2017
Accepted: January 19, 2018
Published: February 15, 2018

REFERENCES

Chang, C.C., Chow, C.C., Tellier, L.C., Vattikuti, S., Purcell, S.M., and Lee, J.J. (2015). Second-generation PLINK: rising to the challenge of larger and richer datasets. Gigascience *4*, 7.

Chen, Y., and Dorn, G.W., 2nd (2013). PINK1-phosphorylated mitofusin 2 is a Parkin receptor for culling damaged mitochondria. Science *340*, 471–475.

Clark, I.E., Dodson, M.W., Jiang, C., Cao, J.H., Huh, J.R., Seol, J.H., Yoo, S.J., Hay, B.A., and Guo, M. (2006). Drosophila pink1 is required for mitochondrial function and interacts genetically with parkin. Nature *441*, 1162–1166.

Frezza, C., Cipolat, S., Martins de Brito, O., Micaroni, M., Beznoussenko, G.V., Rudka, T., Bartoli, D., Polishuck, R.S., Danial, N.N., De Strooper, B., and Scorrano, L. (2006). OPA1 controls apoptotic cristae remodeling independently from mitochondrial fusion. Cell *126*, 177–189.

Greene, J.C., Whitworth, A.J., Kuo, I., Andrews, L.A., Feany, M.B., and Pallanck, L.J. (2003). Mitochondrial pathology and apoptotic muscle degeneration in Drosophila parkin mutants. Proc. Natl. Acad. Sci. USA *100*, 4078–4083.

Greene, A.W., Grenier, K., Aguileta, M.A., Muise, S., Farazifard, R., Haque, M.E., McBride, H.M., Park, D.S., and Fon, E.A. (2012). Mitochondrial processing peptidase regulates PINK1 processing, import and Parkin recruitment. EMBO Rep. *13*, 378–385.

Groth, A.C., Fish, M., Nusse, R., and Calos, M.P. (2004). Construction of transgenic Drosophila by using the site-specific integrase from phage phiC31. Genetics *166*, 1775–1782.

Hackenbrock, C.R. (1966). Ultrastructural bases for metabolically linked mechanical activity in mitochondria. I. Reversible ultrastructural changes with change in metabolic steady state in isolated liver mitochondria. J. Cell Biol. *30*, 269–297.

Hsieh, C.H., Shaltouki, A., Gonzalez, A.E., Bettencourt da Cruz, A., Burbulla, L.F., St Lawrence, E., Schüle, B., Krainc, D., Palmer, T.D., and Wang, X. (2016). Functional impairment in miro degradation and mitophagy is a shared feature in familial and sporadic Parkinson's disease. Cell Stem Cell *19*, 709–724.

Hughes, A.J., Daniel, S.E., Kilford, L., and Lees, A.J. (1992). Accuracy of clinical diagnosis of idiopathic Parkinson's disease: a clinico-pathological study of 100 cases. J. Neurol. Neurosurg. Psychiatry *55*, 181–184.

John, G.B., Shang, Y., Li, L., Renken, C., Mannella, C.A., Selker, J.M., Rangell, L., Bennett, M.J., and Zha, J. (2005). The mitochondrial inner membrane protein mitofilin controls cristae morphology. Mol. Biol. Cell *16*, 1543–1554.

Kazlauskaite, A., Kondapalli, C., Gourlay, R., Campbell, D.G., Ritorto, M.S., Hofmann, K., Alessi, D.R., Knebel, A., Trost, M., and Muqit, M.M. (2014). Parkin is activated by PINK1-dependent phosphorylation of ubiquitin at Ser65. Biochem. J. *460*, 127–139.

Kondapalli, C., Kazlauskaite, A., Zhang, N., Woodroof, H.I., Campbell, D.G., Gourlay, R., Burchell, L., Walden, H., Macartney, T.J., Deak, M., et al. (2012). PINK1 is activated by mitochondrial membrane potential depolarization and stimulates Parkin E3 ligase activity by phosphorylating Serine 65. Open Biol. *2*, 120080.

Körner, C., Barrera, M., Dukanovic, J., Eydt, K., Harner, M., Rabl, R., Vogel, F., Rapaport, D., Neupert, W., and Reichert, A.S. (2012). The C-terminal domain of Fcj1 is required for formation of crista junctions and interacts with the TOB/SAM complex in mitochondria. Mol. Biol. Cell *23*, 2143–2155.

Lajtha, A., Gibson, G.E., and Dienel, G.A. (2007). Handbook of Neurochemistry and Molecular Neurobiology: Brain Energetics. Integration of Molecular and Cellular Processes (Springer).

Lin, C.H., Tzen, K.Y., Yu, C.Y., Tai, C.H., Farrer, M.J., and Wu, R.M. (2008). LRRK2 mutation in familial Parkinson's disease in a Taiwanese population: clinical, PET, and functional studies. J. Biomed. Sci. *15*, 661–667.

Mannella, C.A., Lederer, W.J., and Jafri, M.S. (2013). The connection between inner membrane topology and mitochondrial function. J. Mol. Cell. Cardiol. *62*, 51–57.

Markstein, M., Pitsouli, C., Villalta, C., Celniker, S.E., and Perrimon, N. (2008). Exploiting position effects and the gypsy retrovirus insulator to engineer precisely expressed transgenes. Nat. Genet. *40*, 476–483.

Meeusen, S., DeVay, R., Block, J., Cassidy-Stone, A., Wayson, S., McCaffery, J.M., and Nunnari, J. (2006). Mitochondrial inner-membrane fusion and crista maintenance requires the dynamin-related GTPase Mgm1. Cell *127*, 383–395.

Messerschmitt, M., Jakobs, S., Vogel, F., Fritz, S., Dimmer, K.S., Neupert, W., and Westermann, B. (2003). The inner membrane protein Mdm33 controls mitochondrial morphology in yeast. J. Cell Biol. *160*, 553–564.

Morais, V.A., Haddad, D., Craessaerts, K., De Bock, P.J., Swerts, J., Vilain, S., Aerts, L., Overbergh, L., Grünewald, A., Seibler, P., et al. (2014). PINK1 loss-of-function mutations affect mitochondrial complex I activity via NdufA10 ubiquinone uncoupling. Science *344*, 203–207.

Mun, J.Y., Lee, T.H., Kim, J.H., Yoo, B.H., Bahk, Y.Y., Koo, H.S., and Han, S.S. (2010). Caenorhabditis elegans mitofilin homologs control the morphology of mitochondrial cristae and influence reproduction and physiology. J. Cell. Physiol. *224*, 748–756.

Narendra, D., Tanaka, A., Suen, D.F., and Youle, R.J. (2008). Parkin is recruited selectively to impaired mitochondria and promotes their autophagy. J. Cell Biol. *183*, 795–803.

Ogaki, K., Koga, S., Heckman, M.G., Fiesel, F.C., Ando, M., Labbé, C., Lorenzo-Betancor, O., Moussaud-Lamodière, E.L., Soto-Ortolaza, A.I., Walton, R.L., et al. (2015). Mitochondrial targeting sequence variants of the CHCHD2 gene are a risk for Lewy body disorders. Neurology *85*, 2016–2025.

Park, J., Lee, S.B., Lee, S., Kim, Y., Song, S., Kim, S., Bae, E., Kim, J., Shong, M., Kim, J.M., and Chung, J. (2006). Mitochondrial dysfunction in Drosophila PINK1 mutants is complemented by parkin. Nature *441*, 1157–1161.

Park, Y.U., Jeong, J., Lee, H., Mun, J.Y., Kim, J.H., Lee, J.S., Nguyen, M.D., Han, S.S., Suh, P.G., and Park, S.K. (2010). Disrupted-in-schizophrenia 1 (DISC1) plays essential roles in mitochondria in collaboration with Mitofilin. Proc. Natl. Acad. Sci. USA *107*, 17785–17790.

Parkinson Progression Marker Initiative (2011). The Parkinson Progression Marker Initiative (PPMI). Prog. Neurobiol. *95*, 629–635.

Pesah, Y., Pham, T., Burgess, H., Middlebrooks, B., Verstreken, P., Zhou, Y., Harding, M., Bellen, H., and Mardon, G. (2004). Drosophila parkin mutants have decreased mass and cell size and increased sensitivity to oxygen radical stress. Development *131*, 2183–2194.

Pfanner, N., van der Laan, M., Amati, P., Capaldi, R.A., Caudy, A.A., Chacinska, A., Darshi, M., Deckers, M., Hoppins, S., Icho, T., et al. (2014). Uniform nomenclature for the mitochondrial contact site and cristae organizing system. J. Cell Biol. *204*, 1083–1086.

Pogson, J.H., Ivatt, R.M., Sanchez-Martinez, A., Tufi, R., Wilson, E., Mortiboys, H., and Whitworth, A.J. (2014). The complex I subunit NDUFA10 selectively rescues Drosophila pink1 mutants through a mechanism independent of mitophagy. PLoS Genet. *10*, e1004815.

Poole, A.C., Thomas, R.E., Andrews, L.A., McBride, H.M., Whitworth, A.J., and Pallanck, L.J. (2008). The PINK1/Parkin pathway regulates mitochondrial morphology. Proc. Natl. Acad. Sci. USA *105*, 1638–1643.

Poole, A.C., Thomas, R.E., Yu, S., Vincow, E.S., and Pallanck, L. (2010). The mitochondrial fusion-promoting factor mitofusin is a substrate of the PINK1/parkin pathway. PLoS ONE *5*, e10054.

Rabl, R., Soubannier, V., Scholz, R., Vogel, F., Mendl, N., Vasiljev-Neumeyer, A., Körner, C., Jagasia, R., Keil, T., Baumeister, W., et al. (2009). Formation of cristae and crista junctions in mitochondria depends on antagonism between Fcj1 and Su e/g. J. Cell Biol. *185*, 1047–1063.

Schuldiner, O., Berdnik, D., Levy, J.M., Wu, J.S., Luginbuhl, D., Gontang, A.C., and Luo, L. (2008). piggyBac-based mosaic screen identifies a postmitotic function for cohesin in regulating developmental axon pruning. Dev. Cell *14*, 227–238.

Strauss, M., Hofhaus, G., Schröder, R.R., and Kühlbrandt, W. (2008). Dimer ribbons of ATP synthase shape the inner mitochondrial membrane. EMBO J. *27*, 1154–1160.

Thomas, R.E., Andrews, L.A., Burman, J.L., Lin, W.Y., and Pallanck, L.J. (2014). PINK1-Parkin pathway activity is regulated by degradation of PINK1 in the mitochondrial matrix. PLoS Genet. *10*, e1004279.

Tsai, P.I., Course, M.M., Lovas, J.R., Hsieh, C.H., Babic, M., Zinsmaier, K.E., and Wang, X. (2014). PINK1-mediated phosphorylation of Miro inhibits synaptic growth and protects dopaminergic neurons in Drosophila. Sci. Rep. *4*, 6962.

Tsai, P.I., Papakyrikos, A.M., Hsieh, C.H., and Wang, X. (2017). Drosophila MIC60/mitofilin conducts dual roles in mitochondrial motility and crista structure. Mol. Biol. Cell *28*, 3471–3479.

Valente, E.M., Abou-Sleiman, P.M., Caputo, V., Muqit, M.M., Harvey, K., Gispert, S., Ali, Z., Del Turco, D., Bentivoglio, A.R., Healy, D.G., et al. (2004). Hereditary early-onset Parkinson's disease caused by mutations in PINK1. Science *304*, 1158–1160.

Vives-Bauza, C., and Przedborski, S. (2011). Mitophagy: the latest problem for Parkinson's disease. Trends Mol. Med. *17*, 158–165.

von der Malsburg, K., Müller, J.M., Bohnert, M., Oeljeklaus, S., Kwiatkowska, P., Becker, T., Loniewska-Lwowska, A., Wiese, S., Rao, S., Milenkovic, D., et al. (2011). Dual role of mitofilin in mitochondrial membrane organization and protein biogenesis. Dev. Cell *21*, 694–707.

Wang, X., Winter, D., Ashrafi, G., Schlehe, J., Wong, Y.L., Selkoe, D., Rice, S., Steen, J., LaVoie, M.J., and Schwarz, T.L. (2011). PINK1 and Parkin target Miro for phosphorylation and degradation to arrest mitochondrial motility. Cell *147*, 893–906.

Weihofen, A., Thomas, K.J., Ostaszewski, B.L., Cookson, M.R., and Selkoe, D.J. (2009). Pink1 forms a multiprotein complex with Miro and Milton, linking Pink1 function to mitochondrial trafficking. Biochemistry *48*, 2045–2052.

Whitworth, A.J., and Pallanck, L.J. (2009). The PINK1/Parkin pathway: a mitochondrial quality control system? J. Bioenerg. Biomembr. *41*, 499–503.

Winter, D., Seidler, J., Ziv, Y., Shiloh, Y., and Lehmann, W.D. (2009). Citrate boosts the performance of phosphopeptide analysis by UPLC-ESI-MS/MS. J. Proteome Res. *8*, 418–424.

Woodroof, H.I., Pogson, J.H., Begley, M., Cantley, L.C., Deak, M., Campbell, D.G., van Aalten, D.M., Whitworth, A.J., Alessi, D.R., and Muqit, M.M. (2011). Discovery of catalytically active orthologues of the Parkinson's disease kinase PINK1: analysis of substrate specificity and impact of mutations. Open Biol. *1*, 110012.

Yang, Y., Gehrke, S., Imai, Y., Huang, Z., Ouyang, Y., Wang, J.W., Yang, L., Beal, M.F., Vogel, H., and Lu, B. (2006). Mitochondrial pathology and muscle and dopaminergic neuron degeneration caused by inactivation of Drosophila Pink1 is rescued by Parkin. Proc. Natl. Acad. Sci. USA *103*, 10793–10798.

Yang, Y., Ouyang, Y., Yang, L., Beal, M.F., McQuibban, A., Vogel, H., and Lu, B. (2008). Pink1 regulates mitochondrial dynamics through interaction with the fission/fusion machinery. Proc. Natl. Acad. Sci. USA *105*, 7070–7075.

Yun, J., Puri, R., Yang, H., Lizzio, M.A., Wu, C., Sheng, Z.H., and Guo, M. (2014). MUL1 acts in parallel to the PINK1/parkin pathway in regulating mitofusin and compensates for loss of PINK1/parkin. eLife *3*, e01958.

Ziviani, E., Tao, R.N., and Whitworth, A.J. (2010). Drosophila parkin requires PINK1 for mitochondrial translocation and ubiquitinates mitofusin. Proc. Natl. Acad. Sci. USA *107*, 5018–5023.

STAR★METHODS

KEY RESOURCES TABLE

REAGENT or RESOURCE	SOURCE	IDENTIFIER
Antibodies		
Rabbit anti-dMIC60	This paper	N/A
Rabbit anti-dMIC60p507	This paper	N/A
Rabbit anti-dMIC60p561	This paper	N/A
rabbit anti-TH	EMD Millipore Corporation	AB152; RRID: AB_390204
mouse anti-ATP5β	AbCam	ab14730; RRID: AB_301438
rat anti-Myc	AbCam	ab10910; RRID: AB_297569
mouse anti-V5	Thermo	E10/V4RR; RRID: AB_10977225
mouse anti-GST	Thermo	8-326; RRID: AB_10979611
rabbit anti-dPINK1	Yang et al., 2006	N/A
guinea pig anti-DMiro	Tsai et al., 2014	GP5
rabbit anti-Flag	Sigma	F7425; RRID: AB_439687
rabbit anti-OPA1	Sigma, Poole et al., 2010	M6319; RRID: AB_477221
mouse anti-tubulin	Sigma	T6199; RRID: AB_477583
mouse anti-tubulin	Abcam	ab7291; RRID: AB_2241126
mouse anti-Myc	Santa Cruz	sc-40; RRID: AB_627268
mouse anti-ATP5α	AbCam	ab14748; RRID: AB_301447
Mouse anti-MIC60	Abcam	ab110329; RRID: AB_10859613
Biological Samples		
Human venous blood	National Taiwan University Hospital	N/A
Chemicals, Peptides, and Recombinant Proteins		
TMRM	Molecular Probes	T668
PI	Sigma	P4170
DAPI	Sigma	D9542
Antimycin A	Sigma	A8674
Critical Commercial Assays		
ATP Detection: ATP Determination Kit	Life Technologies	A22066
Experimental Models: Cell Lines		
Human iPSC-derived neurons	XCell Science	Control; PINK1−/−
HEK293T cells	ATCC	CRL-11268G-1
Experimental Models: Organisms/Strains		
dMIC60^{LL02849}	Drosophila Genomics Resource Center, Kyoto, Schuldiner et al., 2008	N/A
PINK1^{PE704}	Clark et al., 2006	N/A
PINK1^{5}	Clark et al., 2006	N/A
PINK1^{RV}	Park et al., 2006	N/A
PINK1^{B9}	Park et al., 2006	N/A
UAS-ND42	Pogson et al., 2014	N/A
UAS-Sicily	Pogson et al., 2014	N/A
UAS-Drp1	Poole et al., 2008	N/A
UAS-MUL1	Yun et al., 2014	N/A
UAS-hPINK1^{WT}-Flag	This paper	N/A
UAS-hPINK1$^{\Delta MTS}$-Flag	This paper	N/A
UAS-dMIC60^{WT}-Myc	Tsai et al., 2017	N/A
UAS-dMIC60^{T507A,T561A}-Myc	This paper	N/A

(*Continued on next page*)

Continued		
REAGENT or RESOURCE	SOURCE	IDENTIFIER
UAS-hMIC60^{WT}-Myc	This paper	N/A
UAS-hMIC60^{A4V}-Myc	This paper	N/A
UAS-hMIC60^{T11A}-Myc	This paper	N/A
UAS-hMIC60^{C17F}-Myc	This paper	N/A
UAS-hMIC60^{R25H}-Myc	This paper	N/A
UAS-hMIC60^{R31C}-Myc	This paper	N/A
Tubulin-GAL4	Lab stock	N/A
Elav-GAL4	Lab stock	N/A
Actin-GAL4	Lab stock	N/A
Da-GAL4	Lab stock	N/A
UAS-mito-GFP	BDSC	8443
UAS-mCD8-RFP	BDSC	27399
Park^{rva}	Greene et al., 2003	N/A
Park^{25}	Greene et al., 2003	N/A
Oligonucleotides		
Please see Table S1		
Recombinant DNA		
pUASTattB-MIC60-Myc	This paper	N/A
pUASTattB-hPINK1-Flag	This paper	N/A
pUASTattB-hPINK1$^{\Delta MTS}$-Flag	This paper	N/A
pGEX6P-1-GST-dMIC60	This paper	N/A
pcDNA3.1-MIC60-Myc, WT, RNAi resistant	This paper	N/A
pcDNA3.1-MIC60-Myc, PR, RNAi resistant	This paper	N/A
pET101-TOPO- dPINK1-His-V5	This paper	N/A
pET101-TOPO- dMIC60-His-V5	This paper	N/A
Software and Algorithms		
PLINK1.9	Chang et al., 2015	N/A

CONTACT FOR REAGENTS AND RESOURCE SHARING

For further information and requests for reagents, please contact Xinnan Wang (xinnanw@stanford.edu).

EXPERIMENTAL MODEL AND SUBJECT DETAILS

Fly Stocks

The following fly stocks were used: Tubulin-GAL4, Actin-GAL4, elav-GAL4, da-GAL4, UAS-mitoGFP, UAS-mCD8RFP (Bloomington *Drosophila* Stock Center, BDSC), *dMIC60^{LL02849}* (*Drosophila* Genomics Resource Center, DGRC, Kyoto) (Schuldiner et al., 2008), *PINK1^{PE704}* (Clark et al., 2006), *PINK1^{5}* (Clark et al., 2006), *PINK1^{RV}* (Park et al., 2006), *PINK1^{B9}* (Park et al., 2006), *Park^{25}* (Greene et al., 2003), *Park^{rva}* (Greene et al., 2003), UAS-ND42 (Pogson et al., 2014), UAS-Sicily (Pogson et al., 2014), UAS-Drp1 (Poole et al., 2008), UAS-MUL1 (Yun et al., 2014). UAS-hPINK1^{WT}-Flag, UAS-hPINK1$^{\Delta MTS}$-Flag, UAS-dMIC60^{WT}-Myc (Tsai et al., 2017), UAS-dMIC60^{T507A,T561A}-Myc, UAS-hMIC60^{WT}-Myc, UAS-hMIC60^{A4V}-Myc, UAS-hMIC60^{T11A}-Myc, UAS-hMIC60^{C17F}-Myc, UAS-hMIC60^{R25H}-Myc, and UAS-hMIC60^{R31C}-Myc were generated using PhiC31 integrase-mediated transgenesis, with an insertion at an estimated position of 25C6 at the attP40 site (BestGene) (Markstein et al., 2008). The age or developmental stage of flies for each experiment was stated in the Figure Legends. Male flies were used for *PINK1* null flies because male *PINK1* null flies are infertile and *PINK1* is on the X chromosome, and an equal number of both male and female flies were used for the other genotypes.

Human Subjects

For the East Asian cohort, 1883 study participants including 250 sporadic early-onset PD patients (onset age < 50 years), 602 sporadic late-onset PD patients (onset age ≥ 50 years), 100 familial PD patients with positive family history (at least one other affected first- and/or second-degree relative with parkinsonism), and 931 age/gender/ethnicity-matched controls, were recruited from the

movement disorder clinic at National Taiwan University Hospital, a tertiary referral center in Taiwan. Among the 100 familial PD patients, 43 followed an autosomal-dominant inheritance pattern, 23 showed autosomal-recessive inheritance, and the remaining 34 had one affected second-degree relative. PD was diagnosed using the UK PD Society Brain Bank diagnostic criteria (Hughes et al., 1992). Unrelated healthy adult volunteers matched for age, gender, and ethnic origins were recruited as controls. Informed consent was obtained from each participant, and the institutional ethics board committees approved this study. DNA extraction from venous blood was performed using standard protocols (Lin et al., 2008). In the first part of the study, complete Sanger sequencing of all the exons and exon-intron boundaries of *MIC60* gene was performed in 250 sporadic early-onset PD patients, 100 probands with positive family history, and 350 age/gender/ethnicity-matched controls. The 15 exons and exon-intron boundaries of *MIC60* gene were amplified using PCR and sequenced by an ABI 3730 analyzer (Applied Biosystems Inc). The primer sequences are provided in Table S1. The multiple ligation probe amplification (MLPA) kits P051 and P052 (MRC Holland, Amsterdam, the Netherlands), covering the exons of *SNCA*, *Parkin*, *PINK1*, *DJ-1*, *ATP13A2*, *PLA2G6*, *FBXO7*, or *DNAJC6*, were used to screen for these genes known to cause familial parkinsonism. Detection of *LRRK2* mutations was described previously (Lin et al., 2008). For the second set of the study, we genotyped the potential pathogenic c.G50T (p.Cys17Phe) substitution using TaqMan Genotyping Assays on a StepOnePlus Real-Time PCR machine (Applied Biosystems Inc) in additional 602 sporadic late-onset PD patients and additional 581 age/gender/ethnicity-matched control subjects. In the first part of the study including 250 sporadic early-onset and 100 probands of familial PD patients, the age of symptomatic onset was 51.3 ± 15.3 years (range, 35–74 years for 203 men and 147 women). In the second part including additional 602 sporadic late-onset PD patients, the onset age was 63.4 ± 7.9 years and 51.2% are men. Both patients harboring p.C17F are male, clinically late-onset, and presented with typical parkinsonian features including a good levodopa response. The familial patient first had progressive asymmetrical rest tremor and slow movement at the age of 61 and had responded well to levodopa for 7 years since onset. The UPDRS part III score was improved from 25 to 8 using levodopa at a dose of 600 mg/day. The sporadic patient first had motor symptoms at the age of 67 and responded well to levodopa. He developed dementia 7 years after motor symptom onset and the MMSE score was 21/30. His head MRI shows diffuse cortical atrophy with slight emphasis on the frontal cortices (Figures S9C and S9D).

The Mayo Clinic PD patient-control cohort consisted of 859 PD patients (age = 76.69 ± 11.11 years; 546 men and 313 women) (Ogaki et al., 2015). The age of symptomatic onset was 65.50 ± 13.08 years (range, 28–97 years). 352 patients had family history and 115 patients presented with early-onset form of the disease (defined as symptomatic onset $\leq$ 50 years). The study included 871 healthy controls (age = 65.08 ± 12.74 years; 374 men and 497 women with no family history of neurodegenerative movement disorders). All subjects included in the study are unrelated, non-Hispanic Caucasians recruited at Mayo Clinic, Jacksonville, USA. Written informed consent was obtained from all participants and the study was approved by all institutional review boards from the participating centers. Both patients harboring the *MIC60* MTS mutants (p.A4V and p.R25H) are late-onset sporadic patients with no recorded family history of the disease.

PPMI is an international, multi-center and progressing study designed to identify PD biomarkers by the Michael J. Fox Foundation (http://www.ppmi-info.org/study-design/). The study design, subject recruitment criteria, site selection, and study assessment have been detailed in (Parkinson Progression Marker Initiative, 2011).

METHOD DETAILS

Generation of dMIC60 Antibodies

Polyclonal dMIC60 antibody was generated by 21st Century Biochemicals (Marlborough, MA) against three peptides of dMIC60 (CAAKPKDNPLPRDVVEL, TASVSDKYWRNVEKARNY, and CLRLKRAIDSVRGDNDS). Phospho-dMIC60 antibodies were generated by Thermo Fisher Scientific (Rockford, IL) against phospho-dMIC60Thr507 (LEDKLA[pT]EKANYK) or phospho-dMIC60Thr561 (ASVRAA[pT]PGVHYK). Antibodies were immuno-depleted against non-phosphorylated peptides.

Constructs

pUASTattB-hMIC60-Myc was generated by cloning human MIC60 from pcDNA3.1-MIC60-Myc (Park et al., 2010) using PCR, engineered with BglII/XbaI restriction sites at either side, into a pUASTattB vector (Groth et al., 2004). pUASTattB-hPINK1-Flag or pUASTattB-hPINK1$^{\Delta MTS}$-Flag was generated by cloning either the full-length human PINK1 cDNA or a fragment encoding AAs 112-581, and the C-terminal Flag, from the hPINK1-Flag construct (Weihofen et al., 2009), engineered with KpnI/XbaI restriction sites at either side, into a pUASTattB vector. Mutant cDNA was generated using site-directed mutagenesis with primers carrying the specific mutations (Table S1). GST-dMIC60 truncated constructs were generated by ligating the PCR-amplified dMIC60 fragments with EcoRI/NotI restriction sites at either side into pGEX6P-1 (GE Healthcare). dMIC60-His-V5 was generated by cloning dMIC60 cDNA into pET101-TOPO (Invitrogen). dPINK1-His-V5 was generated by cloning dPINK1 cDNA, PCR amplified from wild-type (w^{1118}) flies, into pET101-TOPO (Invitrogen).

Analysis of the $\Delta\Psi$m Using TMRM

Third instar wandering larvae were dissected in Schneider's medium (Sigma) with 5 mM EGTA at 22°C in a chamber on a glass slide, then washed and incubated for 20 min with fresh Schneider's medium containing 5 mM EGTA, 20 nM TMRM (Molecular Probes). Next, the solution was replaced with 5 nM TMRM in Schneider's medium for live imaging. For TMRM quantification, the fluorescence

intensity of an individual mitochondrion was normalized to that of the adjacent cytoplasmic region. Six larvae were used for each genotype.

Detection of ATP Level

ATP level was measured using a luciferase-based bioluminescence assay (ATP Determination Kit, Life Technologies) as previously described (Tsai et al., 2014). For each experiment, 5-day-old adult flies were homogenized in 100 μL lysis buffer (6 M guanidine-HCl, 100 M Tris pH 8.0, and 4 mM EDTA). The extracts were boiled for 5 min, placed on ice for 5 min, and centrifuged at 20,000 g for 15 min. The supernatant was then diluted to 1:500 in reaction buffer (provided by the kit) and luciferase was added for 1 min. Luminescence was immediately measured using a Glomax Multi Jr. Reader (Promega). Each reading was normalized to protein concentration measured by bicinchoninic acid (BCA) assay (Thermo Scientific). Five adults were used for each experiment and total there were 6 independent experiments.

Immunocytochemistry and Confocal Microscopy

Adult brains or larval muscles were dissected in PBT (0.3% Tween 20 in PBS), and incubated with fixative solution (4% formaldehyde in PBT) for 20 min, followed by 1 hr blocking with 1% BSA in PBT. Samples were immunostained with rabbit anti-TH (AB152; EMD Millipore Corporation) at 1:200, mouse anti-ATP5β (ab14730; AbCam) at 1:100, rabbit anti-dMIC60 at 1:500, or rat anti-Myc (ab10910; AbCam) at 1:100, and Alexa 488/Cy3/Alexa 647-conjugated anti-rat (ab150165; AbCam)/mouse/rabbit IgG (Fisher) at 1:500. Samples were imaged with a 20 × /N.A.0.60 or a 63 × /N.A.1.30 oil Plan-Apochromat objective on a Leica SPE laser scanning confocal microscope (JH Technologies) with identical imaging parameters among different genotypes in a blind fashion. Images were processed with Photoshop CS4 using only linear adjustment of contrast. For brain imaging, 10-14 brains from 10-14 flies were used. For muscle imaging, 20 images from 4-6 larvae were used.

Mitochondrial Assays

Mitochondria were purified from one hundred 5-day-old adult flies or pupae homogenized in mitochondrial isolation buffer (MIB: 70 mM sucrose, 210 mM Mannitol, 50 mM Tris/HCl pH 7.5, 10 mM EDTA/Tris pH 7.5) with a glass dounce homogenizer, followed by first centrifugation at 600 g for 10 min to remove debris and another centrifugation at 7,000 g for 10 min to pellet mitochondria. Supernatant was saved as "cytosolic fraction." For Proteinase K accessibility assay, isolated mitochondria were treated with 100 μg/ml Proteinase K in MIB at 4°C for 30 min. A hypotonic rupture of the OMM was achieved by resuspensing mitochondria in 2 mM HEPES/KOH pH 7.4. Triton X-100 at a final concentration of 0.3% (v/v) was used to disrupt the IMM. Proteinase K was inactivated by incubating the reaction with 1 mM Pefabloc at 4°C for 5 min. Samples were prepared for SDS-PAGE analysis by precipitation with 10% trichloroacetic acid, followed by cold acetone washes, and resuspension in SDS sample buffer (300 mM Tris/HCl pH 6.8, 25% glycerol, 10% SDS, 0.1% bromophenol blue, and 14.4 mM 2-mercaptoethanol). Samples were run in SDS-PAGE. For dMIC60 oligomerization detection, adult flies were lysed in BN-PAGE sample buffer (Thermo Fisher Scientific) with 1% Digitonin. Samples were run in 3%–12% BN-Bis-Tris-PAGE (Thermo Fisher Scientific). Results were repeated for more than 3 times. For in-gel activity, mitochondrial pellets were resuspended in 200 μL lysis buffer (50 mM NaCl, 50 mM imidazole/HCl pH 7.0, 2 mM 6-amino-caproic acid, and 1 mM EDTA), incubated for 15 min on ice, and solubilized by adding 50 μL 10% dodecylmaltoside (DDM). Mitochondrial fractions were cleared by centrifugation at 16,000 g at 4°C for 30 min, and mixed with 20 μL loading dye (50% glycerol and 0.1% Ponceau S). 50 μg of mitochondrial proteins from each genotype was resolved in a 4%–13% native gel using a cathode buffer (50 mM Tricine, 7.5 mM imidazole, pH 7.0) containing 0.05% (w/v) deoxycholate and 0.01% DDM. Complex I in-gel activity assay was performed by incubating gel strips in complex I reaction buffer (2.5 mg/ml nitrotetrazolium blue, 0.1 mg/ml NADH, and 5 mM Tris/HCl pH 7.4) for 5 min, followed by fixation in 50% methanol and 10% acetic acid. Gels were scanned using a Cannon 5600F scanner for densitometric quantification. For each experiment, 100 adults 5 days after eclosion were used and there were total 4 independent experiments.

Protein Biochemical Assays

dPINK1-His-V5 or dMIC60-His-V5 fusion protein was bacterially expressed, purified by a Ni-NTA column, and eluted with elution buffer (50 mM $NaPO_4$, pH 8.0, 0.3 M NaCl, 250 mM Imidazole). GST-dMIC60 fusion protein was bacterially expressed, purified and immobilized on glutathione beads, and incubated with 5 μg dPINK1-His-V5 protein in NETN buffer (100 mM NaCl, 20 mM Tris at pH 8.0, 0.5% NP40, 0.5 mM EDTA, and PMSF), at 4°C for 2 hr. Co-precipitation complexes were then washed three times with NETN buffer. For *in vivo* immunoprecipitation, mitochondrial fractions isolated from 100 pupae were lysed using NET-2 buffer (50 mM Tris-HCl pH 7.5, 150 mM NaCl, 0.05% NP40) and incubated with 1 μL anti-dMIC60 for 2 hr at 4°C, and then 50 μL 50% washed protein A-Sepharose beads (Amersham) for another 2 hr at 4°C. The beads were then washed three times with NET-2 buffer. The following antibodies were used: mouse anti-V5 (E10/V4RR, Thermo) at 1:2000, mouse anti-GST (8-326, Thermo) at 1:2000, rabbit anti-dPINK1 (Yang et al., 2006) at 1:1000, rabbit anti-dMIC60 at 1:6000, rabbit anti-phospho-dMIC60 at 1:5000, guinea pig anti-DMiro (GP5) (Tsai et al., 2014) at 1:20000, rabbit anti-Flag (F7425; Sigma) at 1:2000, rabbit anti-OPA1–anti-human mitofusion 2, which recognizes *Drosophila* OPA-1 (Poole et al., 2010)–(M6319; Sigma) at 1:1000, mouse anti-tubulin (T6199; Sigma) at 1:3000,

mouse anti-Myc (sc-40; Santa Cruz) at 1:1000, or mouse anti-ATP5α (ab14748; AbCam) at 1:5000, and HRP-conjugated-goat anti-rabbit, guinea pig, or mouse IgG (Jackson ImmunoResearch Laboratories) at 1:5000. Results were repeated for more than 3 times.

TcPINK1 Kinase Assay

TcPINK1 fused with maltose-binding protein (MBP) (Woodroof et al., 2011) was expressed in *E. coli*, purified using amylose resin, and then eluted using kinase assay buffer containing maltose (50 mM Tris–HCl pH 7.5, 0.1 mM EGTA, 10 mM $MgCl_2$, 2 mM dithiothreitol, and 10 mM maltose). Purified TcPINK1 (1 μg) was then incubated with dMIC60-His-V5 (1 μg) in a final volume of 80 μl in kinase assay buffer containing 10 mM ATP at 30°C for 2 hr, and the reaction was terminated by adding SDS sample buffer (300 mM Tris/HCl pH 6.8, 25% glycerol, 10% SDS, 0.1% bromophenol blue, and 14.4 mM 2-mercaptoethanol). Reaction mixtures were resolved either in 7.5% SDS-PAGE then sent for mass spectrometric analysis (see below), or in 6% SDS-PAGE containing 100 μM acrylamide-pendant phos-tag ligand and 100 μM $MnCl_2$ as instructed (http://www.wako-chem.co.jp/english/labchem/product/life/Phos-tag/Acrylamide.htm). Phos-tag containing SDS-PAGE was rinsed in transfer buffer with 1 mM EDTA for 10 min to remove Mn^{2+} before transfer. Phosphatase Inhibitor Cocktail III (524627; Millipore) was applied in all reactions. Results were repeated for more than 3 times except for the mass spectrometry experiment.

Mass Spectrometry

Gel bands were excised, cut to small pieces and transferred into microtubes. In-gel digestion was performed as described elsewhere (Wang et al., 2011). Briefly, gel pieces were destained, and proteins were reduced and alkylated using dithiothreitol and acrylamide prior to trypsin digestion overnight. The next day, peptides were extracted from the gel pieces, dried using a vacuum centrifuge, desalted using C_{18} STAGE tips, dried again, and resuspended in 50 mM citrate (Winter et al., 2009). For LC-MSMS analysis, an Easy-nLC 1000 ultra-high performance liquid chromatography system coupled to an Orbitrap Velos mass spectrometer (both Thermo Fisher Scientific, Bremen, Germany) was used. Analytical columns were self-packed with 5 μm ReproSil-Pur 120 C_{18}-AQ particles (Dr. Maisch, Ammerbuch-Entringen, Germany) using spray tips manufactured from 100 μm inner diameter fused silica capillaries using a P2000 laser puller (Sutter Instruments, Novato, CA, USA). After equilibrating the column with 3 injections of 50 mM citrate, peptide samples were loaded at 1 μl/min in 100% buffer A (water with 0.1% formic acid). After 5 min of washing with the same settings, peptides were eluted with a linear gradient from 100% buffer A to 65% buffer A 35% buffer B (acetonitrile with 0.1% formic acid) in 30 min at a flow rate of 400 nl/min. Eluting peptides were ionized in the positive ion mode using a capillary voltage of 1.6 kV. One survey scan of the intact peptide ions was performed in the Orbitrap part of the mass spectrometer at a resolution of 30,000 followed by MSMS fragmentation of the top 10 most abundant peptide ions in the ion trap part using multi stage activation. Dynamic exclusion was set to 30 s with an exclusion list size of 250. For peptide identification, resulting raw files were processed using Proteome Discoverer 1.4.1. (Thermo Scientific) and searched against Swissprot_2014_01 (http://www.uniprot.org) and cRAP (http://www.thegpm.org/crap) using MASCOT 2.4.1. (http://www.matrixscience.com). Taxonomy was set to *Drosophila* and enzyme specificity to trypsin. Propionamide (cysteine) was selected as fixed modification, and phosphorylation (serine, threonine, and tyrosine) as well as oxidation (methionine) were selected as variable modifications. Mass errors were set to 10 ppm at the MS level and 0.6 Da at the MSMS level. Peptides were filtered at 1% false discovery rate and MSMS spectra of identified phopshopeptides were validated manually. For peptide quantification, extracted ion chromatograms (XICs) of the monoisotopic peak of the respective peptide species (phosphorylated peptides and their unmodified counterparts) were generated, the area under the curve was quantified using Xcalibur 2.2. (Thermo Scientific), and the data was further processed using Microsoft Excel.

Transmission Electron Microscopy

Dissected larvae and adult thoraces were fixed in modified Trump's fixative (0.1 M sodium cacodylate buffer, 1% glutaraldehyde, and 4% formaldehyde) at room temperature (22°C) and kept at 4°C overnight. The fixed specimens were rinsed three times with 0.1 M sodium cacodylate pH 7.4 for 10 min, post-fixed with 0.1 M sodium cacodylate containing 2% osmium tetroxide for 30 min, rinsed three times with 0.1 M sodium cacodylate for 10 min, and finally rinsed five times with ddH_2O for 10 min. For Immuno-gold labeling, third instar larvae were dissected in Schneider's medium with 5 mM EGTA and fixed by pre-fix solution (0.1% glutaraldehyde, 0.1 M sodium cacodylate buffer, 4% formaldehyde, and 2 mM $MgCl_2$) for 1 hr at room temperature. Samples were incubated with rabbit anti-Flag (1:100; F7425, Sigma) overnight at 4°C, followed by incubation with anti-rabbit IgG 1.4-nm samples nanogold (1:50; Nanoprobes) for 1 hr at room temperature and washes with ddH_2O. Samples were then postfixed by Trump's fixative (0.1 M sodium cacodylate buffer, 1% glutaraldehyde, and 4% formaldehyde) for 1 hr at 4°C. The specimens were stained en bloc in 2% aqueous uranyl acetate for 30 min, dehydrated in a graded ethanol series, and subsequently set into Spurr's embedding medium. Thin sections (90 nm) were stained with uranyl acetate and lead citrate, and imaged with a TEM1230 electron microscope (JEOL Company) and a 967 slow-scan, cooled CCD camera (Gatan). Muscles at the A4 segment were sectioned 90 nm apart for 10 consecutive sections starting from the middle line. All TEM images were processed with Photoshop CS4. For TEM quantification, 2-13 images per fly and at least 4 flies per genotype were used.

Behavior Assay

Larval crawling ability was defined as the larva's ability to move from the center of a 55-mm apple agar plate to halfway to the edge (13.75 mm) within 30 s. Climbing ability was defined as the ability of the adult fly to climb 5 cm within 5 s. Jumping ability was defined

as the ability of the adult fly to respond to being tapped in a Petri dish by jumping to right itself. Flying ability was defined as the ability to fly when the dish was turned upside down at 30 cm above a bench. If the fly could accomplish the task, it was given a score of 1; otherwise it was given a score of 0. For behavioral assay, 20-60 flies were used.

Human Cell Experiments

Human iPSC-derived neurons from a healthy subject and the corresponding isogenic *PINK1*−/− were purchased from XCell Science (http://www.xcellscience.com/products/mixed-neurons). The genotypes, gene expression levels, pluripotency, and neuronal identity of these iPSCs and neurons were fully validated by XCell Science. Partially differentiated neurons (7 days *in vitro*) were further differentiated on poly-ornithine and laminin coated Thermanox coverslips (77280; EMS) in a 24-well plate, using Neuro Maturation Media (XCell Science: NM-001-M50) and supplement A (NM-SA) for additional 8 days. This allows more than 90% Tuj1-positive neuronal population according to the manufacture's instruction. HEK293T cells cultured on poly-ornithine and laminin coated Thermanox coverslips were transfected with respective siRNA and RNAi-resistant constructs using calcium phosphate. For MIC60 RNAi, silencer validated siRNA (targeting CACCCAAGCUUUAACCGCATT; S21634, Thermo Fisher Scientific) was applied. A non-targeting siRNA (SIC001, Sigma-Aldrich) with no known mammalian homology was used as a negative control. MIC60 RNAi-resistant pcDNA3.1-MIC60-Myc was generated by substituting the MIC60 RNAi-targeting sequence–CACCCAAGCTTTAACCGCA–with TACACAGGCATTGACTGCA. After transfection for 2 days, cells were fixed for TEM or lysed for western blotting. Neurons and HEK293T cells were fixed with 2% glutaraldehyde and 4% paraformaldehyde in 0.1 M Sodium Cacodylate buffer, pH 7.4 at 4°C overnight. Sample preparation for TEM was performed as described above. For TEM, 30-60 images from 3 independent experiments were used. Cell lysates in the presence of Phosphatase Inhibitor Cocktail III (524627; Millipore) and Protease Inhibitor Cocktail III (539134; Millipore) were incubated with 2 μl anti-Myc (sc-40; Santa Cruz), anti-MIC60 (ab110329; Abcam), or IgG (sc-2025; Santa Cruz) for immunoprecipitation, then run in 35 μM phos-tag or regular PAGE as described above, and blotted with mouse anti-Myc at 1:1000, mouse anti-MIC60 at 1:500, or mouse anti-tubulin (ab7291; Abcam) at 1:3000. For calf intestinal alkaline phosphatase (CIP) reactions, no phosphatase inhibitors were used, but the immunoprecipitates were incubated with either 5 μL or 20 μL of CIP (M0290; New England Biolabs) in a buffer (100 mM NaCl, 50 mM Tris-HCl, 10 mM $MgCl_2$, and 1 mM dithiothreitol) at 37°C for 1 hr. Results were repeated for more than 3 times. For neuronal sensitivity, neurons were transfected with EGFP and treated with Antimcin A as previously described (Hsieh et al., 2016). Briefly, culture medium was replaced with Opti-MEM (GIBCO) prior to transfection. 0.5 μg of DNA or 5 μL of Lipofectamine 2000 was diluted in Opti-MEM at room temperature (22°C) to a final volume of 50 μL in two separate tubes, and then contents of the two tubes were gently mixed, incubated for 20 min at room temperature and subsequently added onto neurons. After transfection for 6 hr, DNA complexes in Opti-MEM were replaced with regular N2 medium. Antimycin A (A8674; Sigma-Aldrich) was applied to neurons at 10 μM. For neuronal sensitivity, 30 imaging fields from 3 independent transfections were used. PI (P4170; Sigma) at 2.5 μg/ml, and 4', 6-Diamidino-2-phenylindole (DAPI–D9542; Sigma) at 0.5 μg/ml were applied at room temperature in the dark for 10 min to HEK cells. For HEK cell sensitivity, 15 imaging fields from 3 independent transfections were used. Samples were imaged at room temperature with a 20 × /N.A.0.60 or a 63 × /N.A.1.30 oil Plan-Apochromat objective on a Leica SPE laser scanning confocal microscope (JH Technologies), with identical imaging parameters among different genotypes in a blind fashion. Images were processed with ImageJ (Ver. 1.48, NIH) using only linear adjustments of contrast and color.

QUANTIFICATION AND STATISTICAL ANALYSES

Throughout the paper, the distribution of data points is expressed as box-whisker plots, except otherwise stated. The One-Way ANOVA Post hoc Tukey test was performed for comparisons among multiple groups. The Mann-Whitney *U* test was performed for comparisons between two groups. The Chi Square Test was performed for behavioral tests. Human genetic association tests were performed by logistic regression, adjusting for age and sex. Meta-analysis was carried out in PLINK1.9 (Chang et al., 2015). For all experiments, between 3 and 60 animals or independent experiments were used. The number of animals and experimental replications (n) can be found in the Figure Legends and Method Details. No statistical methods were used to predetermine sample sizes, but the number of flies, experiments and biological replicates were chosen based on the nature of the experiments (it is usually difficult to assess an outcome that follows a normal distribution in our experiments), degree of variations, and published papers describing similar experiments (for example Morais et al., 2014; Poole et al., 2010; Pogson et al., 2014). We did not exclude any data. * $p < 0.05$, ** $p < 0.01$, *** $p < 0.001$ for all figures.